PHYSICS-BASED UNCERTAINTY QUANTIFICATION FOR ZRH$_X$ THERMAL SCATTERING LAW

A Thesis

by

WEIXIONG ZHENG

Submitted to the Office of Graduate and Professional Studies of
Texas A&M University
in partial fulfillment of the requirements for the degree of

MASTER OF SCIENCE

Chair of Committee,	Ryan G. McClarren
Committee Members,	Marvin L. Adams
	Bani Mallick
Head of Department,	Yassin A. Hassan

December 2013

Major Subject: Nuclear Engineering

ABSTRACT

The thermal neutron scattering cross sections of ZrH_x are heavily affected by the solid frequency distributions, also called "phonon spectra", of Zr and H in ZrH_x. The phonon spectra are different for ZrH_x with different x. While current reference data files, e.g. ENDF, are based on the spectra of ZrH_2. This may induce unneglible errors in the simulations for TRIGA reactor. We, therefore, proposed parameterized phonon spectra that can explore the effects of changing the spectra by varying the parameters. For example, we can shift the phonon positions in the spectra. The ultimate goal of this type of work is to calibrate appropriate parameter sets to improve the simulation accuracy via comparing the simulation results and experimental data.

In this thesis, a code has been developed to process the thermal scattering data for transport codes to use. Inputs of the code is basically the proposed parameters. The accuracy of the code processing Legendre moments of scatteirng were demonstrated.

NJOY and MCNP were used to carry out the data processing and neutronic simulations, respectively. The phonon spectra were generated with the parameters produced in Latin Hypercube sampling designs. Quantities, like reactivity (ρ), fission rate density (FRD), neutron mean generation time (Λ), fuel temperature feedback coefficient (α_T^{Fuel}), effective delayed neutron fraction (β_{eff}) and ex-core detector material absorption rate (R_{abs}), were analyzed. Analyses indicate that ρ, Λ and α_T^{Fuel} are sensitive to the variations of parameters. Explicit relationships were established for those quantities and the parameters. However, FRD and R_{abs} is insensitive to any parameters. β_{eff} are sensitive to the parameterized models, however, no explicit relationship could be built due to the unrecognized nonlinearities.

Ongoing work will perform these analyses for the state near critical. Furthermore,

time-dependent behavior could be investigated and when combined with experimental data the reasonably accurate phonon spectrum models and therefore $S(\alpha,\ \beta)$ tables for the TRIGA reactor at Texas A&M University would be produced.

ACKNOWLEDGEMENTS

TABLE OF CONTENTS

LIST OF FIGURES

I. INTRODUCTION: THE IMPORTANCE OF THERMAL SCATTERING FROM ZrH$_x$

In TRIGA reactors, such as the Texas A&M University, Nuclear Science Center reactor, U-ZrH$_x$ is used as the fuel material taking the advantage of the large prompt negative temperature coefficient of reactivity and good moderation of the hydrogenous solid.

In fast and epithermal ranges, the simple two-body scattering model is used for hydrogen and zirconium. However, at thermal energy, things become complicated. When the incident neutrons are thermal, energy of which is comparable with the energy of bindings of the solid, the scattering is heavily affected by the binding forces in the bound system of ZrH$_x$, i.e. affected by the frequency distributions, also called phonon spectra, of the solids.

For thermal neutrons, the double differential scattering cross section is given by

$$\sigma(E' \rightarrow E, \mathbf{\Omega'} \cdot \mathbf{\Omega}) = \frac{\sigma_b}{4\pi kT}\sqrt{\frac{E}{E'}}S(\alpha, \beta), \tag{1.1}$$

where E' and E are the incident and secondary neutron energies. The $S(\alpha, \beta)$ is called the thermal scattering law. The definitions of α and β are:

$$\alpha \equiv \frac{E + E' - 2\mu\sqrt{EE'}}{AkT} \quad \text{and} \quad \beta \equiv \frac{E - E'}{kT} \tag{1.2}$$

α and β are the momentum and energy transfer, respectively. A is the ratio of scatterer mass to neutron mass. With the Gaussian approximation[2] the scattering

1

law can be expressed as:

$$S(\alpha, \beta) = \frac{1}{2\pi} \int\limits_{-\infty}^{\infty} e^{i\beta\hat{t}} e^{-\gamma(\hat{t})} dt \qquad (1.3)$$

where $\hat{t}$ is a non-dimensional time which is measured in the units of $\hbar/kT$. $\gamma(\hat{t})$ is given by

$$\gamma(\hat{t}) = \alpha \int\limits_{-\infty}^{\infty} \frac{\rho(\beta)}{2\beta \sinh(\beta/2)} \left[1 - e^{-i\beta\hat{t}}\right] e^{-\beta/2} d\beta \qquad (1.4)$$

where $\rho(\beta)$ is the phonon spectrum of the bound system in terms of the energy transfer. From Eq. 1 through Eq. 4, we notice that the phonon spectrum contains all the information needed to calculate the scattering law, so as to calculate the scattering cross sections. Therefore, specifying a phonon spectrum is, in some sense, equivalent to specifying a scattering law, and then the scattering cross sections.

In practice, however, the phonon spectra cannot be exactly specified due to the uncertainty of solid structure.

Currently, the tabulated scattering law data of both H and Zr in ZrH_x in ENDF are calculated by using the phonon spectra developed by Slaggie (1968) based on the central force model (CF) for ZrH_2 [4]. In this model, ZrH_2 is assumed to have the face centred cubic (fcc) lattice structure (δ-phase), while for x around 2 the solid is actually the pure face centred tetrangonal (fct) lattice structure (ϵ-phase) [8]. And the lattice structure changes when x changes. One example is ZrH ($x = 1$) is a mixture of α, δ and γ phase lattice. In a word, the lattice structure appears to be dependent on the H concentration. Total cross section measurements reported by Podewils, et al. lend support to this statement [7]. Double differential scattering cross section measurements for multiple x values done by Couch, et al. also appears to indicate the dependency. The phonon spectrum is said to be affected by the lattice

2

structure type [4]. Therefore, for a real TRIGA reactor, with arbitrary x (less than 2), the phonon spectra must be different from the one from ENDF.

On one hand, the scattering law can be specified by specific phonon spectrum; on the other hand, the thermal scattering cross sections, which would affect neutronic simulations, is related directly with the scattering law. Hence the criticality should be affected by varying the phonon spectra.

The facts above inspires one to develop parameterized phonon spectrum models such that corresponding scattering laws could be applied in the simulations and the explicit relationships between the parameters and quantities of interest (QOIs) in the simulations could be establised such that uncertainties of QOIs due to the uncertainty of the spectra would be quantified. This uncertainty quantification (UQ) research is expected to help improve the accuracy of NSC reactor simulations.

Specifically, this thesis will illustrate the following work in this UQ study

1. The developed code to process the scattering cross sections with the parameterized phonon spectrum models and its verification;

2. The UQ study on the variations of QOIs due to the variations of the parameters of the parameterized models based on semi-infinite lattice model of TRIGA reactor;

3. The UQ study on the variations of QOIs due to the variations of the parameters of the parameterized models based on full-core model of TRIGA reactor.

1.1   Parameterized Models of Phonon Spectra

Previous work studied the details of the phonon spectra of ZrH_x. Here we give a brief summary of the works on modeling spectra: Slaggie assumed a fcc model for ZrH_2 and derived phonon spectra, which are applied in ENDF, with the solid physics

code GASKET [12, 6]. Mattes, et al. did new evaluations with the derivation of Debye-plus-Gaussian phenominalogical model (DG) for H in ZrH_x with the free-gas treatment for Zr in ZrH_x [8]. Malik, et al. derived a three-Gaussian model for the optical part of the H spectrum for $ZrH_{1.58}$ [7]. Evans, et al. derived the optical part of the H spectrum in a reverse way by deriving from the measured scattering law [3].

The parameterized models in this thesis rose from Mattes, et al's. work on tabulating the scattering law with the DG model. The DG model, similar with CF model, is based on the assumption that the molecule has a fixed phonon state. Nevertheless, the DG model still has benefit of agreeing well with experiments despite its simple form consisting of Debye and Gaussian distributions. This fact inspired us to develop a similar parameterized mathematical model for the H part of the spectrum and use simple parameterized curves that have similar shapes with the Zr spectrum in CF model to represent our model for Zr in ZrH_x. Eventually, a four-parameter model for H and a three-parameter model for Zr in ZrH_x were developed.

1.2   Code-to-code Comparisons for the Code

There were two ways of carrying out the simulations: one way was to use our code to generate multigroup Legendre moments of thermal scattering of ZrH_x and use PDT, the S_N code developed at Texas A&M University, to take the neutronic simulations; the other was to process data with NJOY and run the simulations with MCNP. Though the latter one was eventually selected, the code generating PDT-compatible data has already been developed. Therefore, we still presents its verification in this thesis.

A key point of calculating the scattering law is how the integration in Eq. 3 is resolved. Thus the phonon expansion was introduced [2]. The original intention of developing the code was such that it could process multigroup thermal scattering

data for transport code, to carry out the criticality calculations. Verification of the code was performed by taking code-to-code comparisons with the THERMR module of NJOY. Quantities, such as $\bar{\mu}$ and $\sigma(E' \rightarrow E)$ were calculated with some common set of parameters. The parameterized models demonstrate good agrement with NJOY calculations.

1.3   Neutronics Simulations for Lattice Model

We eventually determined to use NJOY with MCNP to do the UQ research. NJOY is capable of processing thermal scattering data compatible with MCNP. In this thesis, several modules were invoked such that once the phonon spectra were prepared for the LEAPR module in NJOY, continuous-energy (CE) thermal scattering cross section data compatible with MCNP can be generated.

Parameters are given in some specific ranges. Some were suggested by previous work [12], while some ranges were determined by numerical limitations. More details are discussed in Chapter. 3. The Latin Hypercube sampling was enagaged for sampling the parameter sets. Each parameter was uniformly distributed in the corresponding interval. And then NJOY took those parameters and MCNP thereafter archived CE data.

QOIs extracted from the lattice simulation was believed to tell one about the efficacies of the methods and the sensivity of the QOIs to the parameters. In the lattice simulations, the reactivity (ρ) of the lattice and the fission rate density (FRD) were selected as QOIs.

We aimed to find the main factors based on our parameterized models. There are several ways to archive the goals [11]. The analysis of variance (ANOVA) is one of them. We used the ANOVA to determine the significance of each parameter and regressions to establish simple explicit relatioinships between the QOIs and the

pricipal factors indicated by the ANOVA. Cross validations were used to test if the regression model were reasonable. Results from ANOVA show reactivity is sensitive to two of the seven parameters while FRD is insensitive to any of the parameters; cross validations show good agreement between the predictions from linear regression and the simulation results for reactivity. While FRD behaves as a constants with random noise.

The work in the lattice model simulations indicate the peasibility of the ANOVA-regression-cross validation chain and inspired one to find more QOIs sensitivity to the parameters in the full-core analyses.

1.4   Neutronics Simulations for Full-core Model

In Slaggie's paper, the lattice dynamics simulations for ZrH_2 show three peaks in the optical part around 130 meV, 137 meV and 150 meV, respectively [12]. While for our parameterized model, the optical peak position is centered at 137 meV with a range of 5 meV. This indicate we would need to extend the range of the optical peak position. Moreover, Badea shifted the optical part of CF model by ± 10 meV and observed large effects on the k_{eff} and $\frac{dk_{\text{eff}}}{dT}$ [1]. Therefore we did the extension for the optical peak position to [127, 147] meV.

We took over 5000 MCNP simulations for the full-core TRIGA model to archive the QOIs: reactivity ρ, neutron mean generation time Λ, fuel temperature coefficient α_T^{Fuel} and delayed neutron fraction β. Analyses show that ρ and Λ are sensitive to some factors while the other two are insensitive to any parameter, even though β varies from 0.0060 to about 0.01.

Moreover, 100 MCNP simulations were taken for tallying the absorption rate ex-core detectors. Results did not indicate sensitivities to the parameterized phonon spectra.

1.5   Synopsis

This thesis begins with theory and algorithms to calculate the thermal scattering cross section and the scattering law in Chapter 2. Chapter 3 presents the verification for the code developed for processing thermal scattering cross section of ZrH_x based on the theory and algorithms provided in Chapter 2. Chapter 3 is the verification for the developed code to process thermal scattering data of ZrH_x. In Chapter 4 and 5 the analyses for the relationship between parameters and QOIs for lattice and full-core TRIGA reactor model. Chapter 6 is the conclusions and indications for future work.

II.   THEORY AND ALGORITHMS

In the bound system of ZrH_x, two types of scattering are concerned at thermal energies: incoherent inelastic scattering and incoherent elastic scattering. Coherent scattering, an important phenomenon in crystalline solids (e.g. graphite) but not in hydrogenous solids, e.g. ZrH_x [6], is not included in this study.

2.1   Incoherent Inelastic Scattering

In Chapter 2, the connexion between the scattering law and the phonon spectrum has been given. Define an intermediate function $P(\beta)$.

$$P(\beta) = \frac{\rho(\beta)}{2\beta \sinh(\beta/2)}, \tag{2.1}$$

then Eq. 1.4 can be rewritten as:

$$\gamma(t) = \alpha \int_{-\infty}^{\infty} d\beta \, P(\beta) \left[1 - e^{-i\beta t}\right] e^{-\beta/2} \tag{2.2}$$

Actually, there are some constraints for the spectrum:

$$\int_{0}^{\infty} \rho(\beta)d\beta = 1, \quad \rho(\beta) = \rho(-\beta), \quad \text{and} \quad \lim_{\beta \to 0} \rho(\beta) = \beta^{\zeta}, \tag{2.3}$$

with $\zeta = 2$ [8]. The first constraint is to keep the spectrum normalised; the last constraint is made to guarantee the existence of the limit $\lim_{\beta \to 0} P(\beta)$ such that the integral in Eq. 1.4 holds. In this work an extention has been made such that ζ can be larger than 2 for Zr part. In Mattes's evaluation, Zr in ZrH_x is treated as free

gas [8], the free-gas approximation is given by:

$$S(\alpha, \beta) = \frac{1}{\sqrt{4\pi\alpha}} \exp\left[-\frac{(\alpha + \beta)^2}{4\alpha}\right] \tag{2.4}$$

In order to simplify the Fourier transform in Eq. 4, the "Phonon expansion" is introduced as illustrated in Eq. 2.5. The key is to expand the exponential term with:

$$e^{\gamma(t)} = e^{-\alpha\lambda} \sum_{n=0}^{\infty} \frac{1}{n!} [\gamma(t)]^n, \tag{2.5}$$

where λ is the Debye-Waller integral and is presented as:

$$\lambda = \int_{-\infty}^{\infty} P(\beta) d\beta. \tag{2.6}$$

Then the scattering law can be rewritten as:

$$S(\alpha, \beta) = e^{-\alpha\lambda} \sum_{n=0}^{\infty} \frac{1}{n!} \alpha^n \frac{1}{2\pi} \int_{-\infty}^{\infty} e^{i\beta t} \gamma(t)^n dt \tag{2.7}$$

Define the Fourier transform term to be $\lambda^n T_n(\beta)$ and rewrite the equation above as:

$$S(\alpha, \beta) = e^{-\alpha\lambda} \sum_{n=0}^{\infty} \frac{1}{n!} \alpha^n \lambda^n T_n(\beta) \tag{2.8}$$

where

$$T_0(\beta) = \frac{1}{2\pi} \int_{-\infty}^{\infty} e^{i\beta t} dt = \delta(\beta) \tag{2.9}$$

and

$$T_1(\beta) = \int_{-\infty}^{\infty} e^{i\beta t} \frac{\gamma(t)}{\lambda} d\beta = \frac{\rho(\beta) e^{-\beta/2}}{2\lambda\beta \sinh(\beta/2)} = \frac{P(\beta) e^{-\beta/2}}{\lambda} \tag{2.10}$$

9

In order to calculate higher-order $T_n(\beta)$, the convolution is used:

$$T_n(\beta) = T_1(\beta) * T_{n-1}(\beta) = \int_{-\infty}^{\infty} T_1(\beta')T_{n-1}(\beta - \beta')d\beta'. \tag{2.11}$$

Given β grids, the $T_n(\beta)$ functions are computed for n up to a maximum number, typically 100 [6]. And when tabulating the scattering law, the zero-phonon term, the delta function, should be carried out seperately. Physically, this term is accounting for the incoherent elastic scattering, which will be introduced in the following section.

For thermal neutrons with relatively high energy, e.g. several eV, thermal effects would not be ignored. However, for neutrons with such high energy, the maximum order truncating the series in Eq. 2.5 needs to be large to keep the accuracy [6]. In the LEAPR module in NJOY, the short-collision-time approximation (SCT) is used instead. It is given by

$$S(\alpha, \beta) = \frac{1}{4\pi\alpha\bar{T}/T} \exp\left[-\frac{(\alpha + \beta)^2}{\alpha\bar{T}/T}\right] \tag{2.12}$$

where $\bar{T}$ is the effective temperature and is given by

$$\bar{T} = \frac{T}{2\pi} \int_{-\infty}^{\infty} \beta^2 P(\beta)e^{-\beta}d\beta \tag{2.13}$$

2.2 Incoherent Elastic Scattering

With the zero-phonon term in the phonon expansion, the double differential scattering cross section of the incoherent elastic scattering can be expressed as:

$$\sigma(E' \to E, \mathbf{\Omega}' \cdot \mathbf{\Omega}) = \frac{\sigma_b}{4\pi kT}\sqrt{\frac{E}{E'}}\delta(\beta) \tag{2.14}$$

And then it is straightforward to derive the differential scattering cross section

$$\sigma^{\text{iel}}(E', \mathbf{\Omega}' \cdot \mathbf{\Omega}) = \frac{\sigma_b}{4\pi} e^{-2WE'(1-\mu)}, \tag{2.15}$$

where W is the Debye-Waller coefficient and is given by

$$W = \frac{\lambda}{AkT} \tag{2.16}$$

And the total scattering cross section would be

$$\sigma^{\text{iel}}(E) = \frac{\sigma_b}{2} \frac{1 - e^{-4WE}}{2WE}. \tag{2.17}$$

2.3   Quantities for Verifications

In the following chapter, some quantities are calculated by our code and used to compare with NJOY. They include $\sigma(E' \rightarrow E)$ (with units of b/meV), $\bar{\mu}$, $S(\alpha, \beta)$, etc.

It is direct to calculate $\sigma(E' \rightarrow E)$ from $\sigma(E' \rightarrow E, \mathbf{\Omega}' \cdot \mathbf{\Omega})$ via integrating over directions.

$$\sigma(E' \rightarrow E) = \int_0^{2\pi} d\gamma \int_{-1}^{1} d\mu \, \sigma(E' \rightarrow E, \mathbf{\Omega}' \cdot \mathbf{\Omega}) \tag{2.18}$$

In the calculation of $\bar{\mu}$, the scattering cross sections are used as weighting functions as follow:

$$\bar{\mu} = \frac{\int_0^{E_{th}} dE \int_{-1}^{1} d\mu \, \mu \sigma(E' \rightarrow E, \mathbf{\Omega}' \cdot \mathbf{\Omega})}{\int_0^{E_{th}} dE \int_{-1}^{1} d\mu \, \sigma(E' \rightarrow E, \mathbf{\Omega}' \cdot \mathbf{\Omega})} \tag{2.19}$$

The multigroup Legendre moments are also used in the code-to-code comparisons.

The moments are given by:

$$\sigma_{l,g'\to g} = \frac{\int\limits_{g'} dE' f_l(E') \int\limits_{g} dE \, \sigma_l(E' \to E)}{\int\limits_{g'} dE' f_l(E') \int\limits_{g} dE}, \tag{2.20}$$

where

$$\sigma_l(E' \to E) = \int\limits_{0}^{2\pi} d\gamma \int\limits_{-1}^{1} d\mu \, P_l(\mu)\sigma(E'\to E, \mathbf{\Omega'} \cdot \mathbf{\Omega}). \tag{2.21}$$

l is the order of the moment, $f_l(E)$ is the weighting function, g' and g are the group numbers of incident and outgoing neutrons, respectively, and $P_l(\mu)$ is the zonal Legendre polynomial. Actually, for TRIGA reactors, the weighting function can simply be Maxwellian spectrum and this should not introduce much error if subgroups are fine enough when doing the group collapse:

$$f_l(E) = \frac{E}{(kT)^2} \exp\left(-\frac{E}{kT}\right). \tag{2.22}$$

With this simple weighting function, fortunately, an analytical benchmark for testing the code could be generated.

2.4   Phonon Spectra

In this thesis, parameterized phonon spectra were constructed by some simple math functions with seven adjustable parameters.

The fact that the DG model agreeing well with experiments inspired us to build the parameterized model for H in ZrH_x based on it.

For H, we modified the acoustic part of the DG model of H such that the shape of that part is more like the one from CF model. In this tiny bit modification, the magnitude of the acoustic Debye distribution is lowered to the half and mirrored

about the Debye temperature such that it looks more like the CF model, from lattice dynamics calculation, and simulataneously keeps the same branching ratio of the acoustic part as the value suggested by Mattes [8]. And that is the reason of the existence of two quadratic equations in Eq. 2.23.

For Zr, Slaggies suggested a Debye distribution with the Debye temperature of 20 meV as the simplification of the CF model [12]. Mattes, et al. proposed to use the free-gas treatment [8]. In order to make the new spectrum flexible, wo use neither the free-gas model, nor the Debye distribution. Instead, some modifications were done to Slaggie's Debye distribution. We still keep the power function shape on the left of the Debye temperature, while the power is changed from 2 to a variable larger than 2. This does not break the constraint mentioned in Eq. 2.3. On the right part, we expected a function attenuating with a limit of zero when the energy transfer, β, increases. Then we came up with the exponential function, shown in Eq. 2.24, due to its fast attenuation and integrability.

Figure 2.1 shows the reference phonon spectra for H and Zr[8, 6]. Note that, in this thesis, IKE and ENDF stand for different libraries. When they appear in this thesis, they represent the DG model and CF model, respectively.
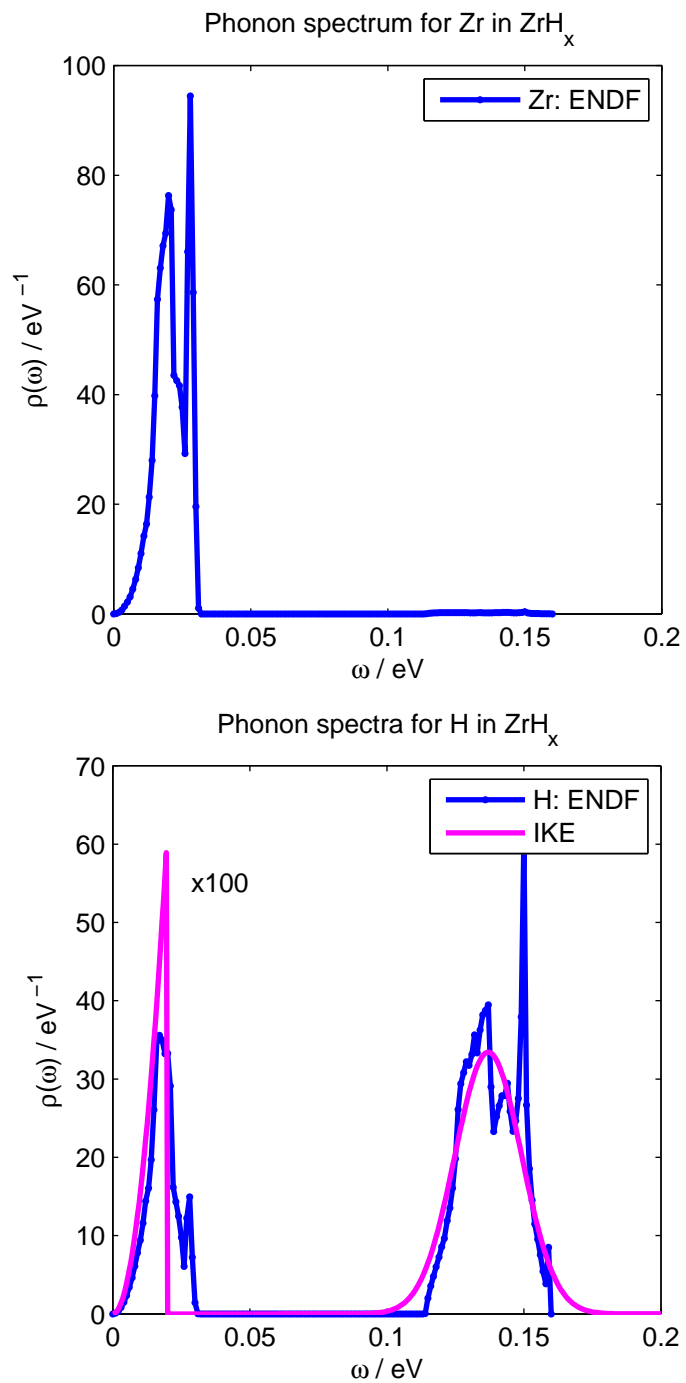
Figure 2.1: Reference spectra for Zr and H in ZrH_x.

For H, the model is:

$$\rho(\omega)_{\mathrm{H}} = \begin{cases} \dfrac{3b}{2T_{\mathrm{DH}}^3}\omega^2 & \omega < T_{\mathrm{DH}} \\[3ex] \dfrac{3b}{2T_{\mathrm{DH}}^3}(\omega - 2T_{\mathrm{DH}})^2 & T_{\mathrm{DH}} \le \omega \le 2T_{\mathrm{DH}} \\[3ex] \dfrac{c(b)}{\sqrt{2\pi}\sigma}\exp\left[-\dfrac{(\omega - p)^2}{2\sigma^2}\right] & 2T_{\mathrm{DH}} \le \omega \le \omega_{\mathrm{max,H}}. \end{cases} \tag{2.23}$$

For Zr, the spectrum is given by:

$$\rho(\omega)_{\mathrm{Zr}} = \begin{cases} \dfrac{r(1+c)}{T_{\mathrm{DZr}}^{1+c}}\omega^c & \omega < T_{\mathrm{DZr}} \\[3ex] \dfrac{(1+c)r}{T_{\mathrm{DZr}}}\exp\left[\dfrac{(1+c)^r}{1-r}\left(1 - \dfrac{\omega}{T_{\mathrm{DZr}}}\right)\right] & T_{\mathrm{DZr}} \le \omega \le \omega_{\mathrm{max,Zr}}. \end{cases} \tag{2.24}$$

In Eq. 2.23, b is the branching ratio of the acoustic part; T_{DH} is the Debye temperature of H in ZrH_x; p is the peak position of the optical part of the spectrum, which is also the mean of the Gaussian distribution, the optical part; σ, which is calculated from the given FWHM of the optical part, is the standard deviation of the Gaussian distribution. Figure 2.2 and Figure 2.3 are examples of how the parameterized models of H and Zr in ZrH_x behave by varying parameters. In these figures, the "Case" numbers are the ordering numbers in the 3000-set LHS design.
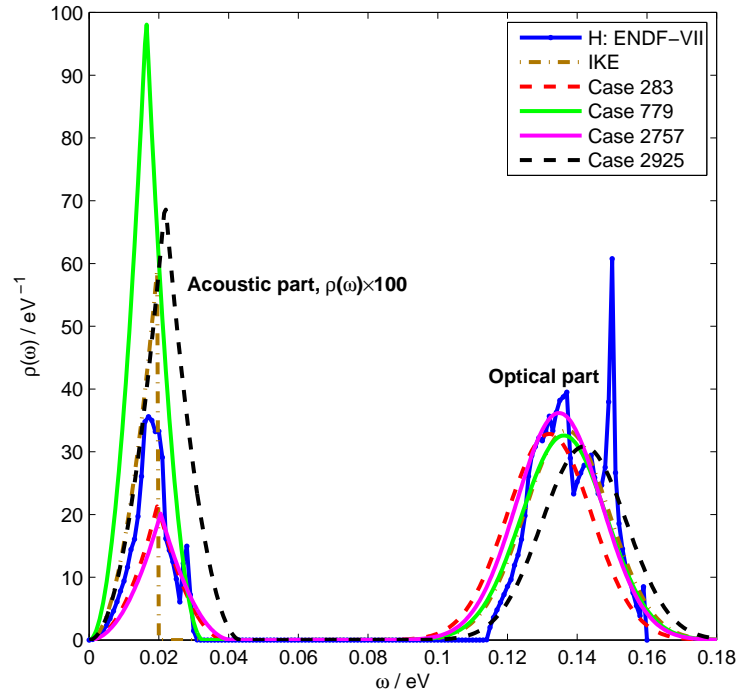
Figure 2.2: Comparisons between the reference spectra and the parameterized spectra for H in ZrH_x.
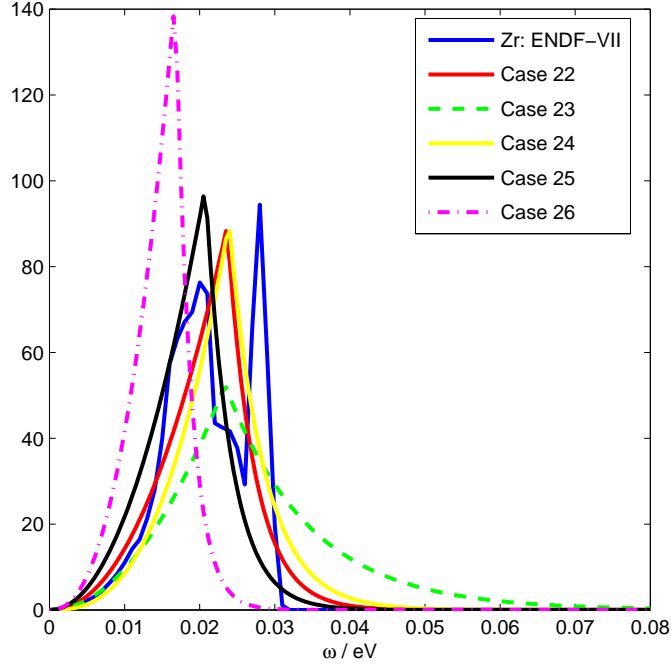
Figure 2.3: Comparisons between the reference spectra and the parameterized spectra for Zr in ZrH_x.

In Eq. 2.24, T_{DZr} is the peak position of the Zr spectrum; c is the power of ω for the left side of the peak; r is the ratio of the left part of the peak to the whole spectrum. Overall, in the parameterized model of spectra of ZrH_x, there are seven parameters: b, T_{DH}, p, FWHM, T_{DZr}, c and r.

For the H part, in the DG model, Mattes suggested that b, T_{DH}, p and FWHM take 1/241, 20 meV, 137 meV and 28 meV, respectively. Supported by Evans, et al.'s work that for different type of ZrH_x solids the spectra change, ranges of [16, 24]meV and [25, 31]meV were set for T_{DH} and FWHM, respectively. Slaggie's lattice dynamics simulation results for ZrH_2 suggested a range of [1/361, 1/91] for b. The range of

p was originally set as [132, 142] meV for the TRIGA fuel lattice simulations, and was enlarged to [127, 147] meV inspired by Slaggie's and Badea's work [1, 12].

For the Zr part, the ranges of r, c and T_{DZr} were set as [0.4, 0.8], [2, 2.8] and [16, 24] meV, respectively. Theoretically, the limit of r, which is 1, is the situation suggested by Slaggie's simple Debye distribution, whatever c is if the Debye temperature is set as 20 meV. However, when implementing the model on MATLAB, there are numerical limitations around 0.8 for r and 2.8 for c such that the Debye-Waller integral in Eq. 2.6 could not be resolved if corresponding parameters are beyond those limitations. And the lower bound of c is simply the constraint mentioned in Eq. 2.3. Figure 2.4 presents $\rho(\beta)$ vs. β and $P(\beta)$ vs. β when $c = 2.8$ and $r = 0.8$. It can be seen that the right part of the Debye temperature is sharp. Actually, it was sharp enough to make the integrators fail. Moreover, these two parameters were proposed not because there are some physical bases behind them, but we aimed to make the spectrum resonably flexible and able to mimic the spectrum of Zr in ZrH_x in some senses.
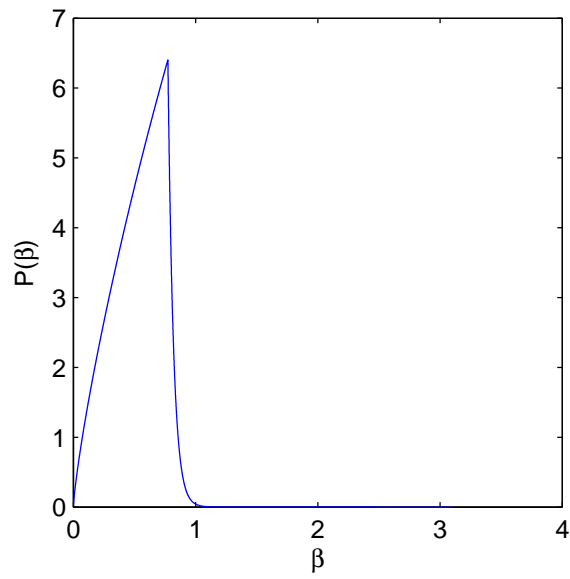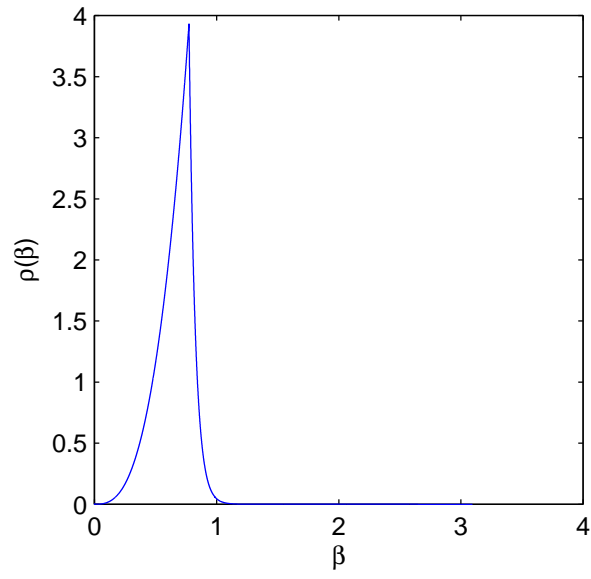
Figure 2.4: $\rho(\beta)$ and $P(\beta)$ when c and r reach their limitations.

III.   CODE TO CODE COMPARISON

We have developed a code to process thermal scattering cross sections for ZrH_x, as a function of the parametersmentioned in the previous chapter. This will be used in simulations of time dependent behavior of the core using PDT in the future.

3.1   The Code and Choice of the Parameters

The code is currently built on MATLAB platform with parallel capability (using matlabpool). As originally expected, it was built such that only seven parameters are needed to take the cross section processing. The code consists of several modules accounting from generating phonon spectra through calculating thermal multigroup scattering Legendre moments.

For H, with a common set of parameters, some quantities were calculated using our code for testing purposes. The parameters for H are from the values based on Mattes, et al. [8]. The parameters for Zr, unfortunately, do not have such reference. In this chapter, the Zr parameters were selected randomly from a LHS design based on the ranges for c, r and T_{DZr}. This selection has the c of 2.014, r of 0.646 and T_{DZr} of 17 meV.

Simultaneously, NJOY was used to carry out the same tasks with ENDF scattering law data generated from Slaggie's CF model as comparisons.

3.2   Testing Quantities and Results

3.2.1   Testing Quantities

For the purpose of testing both the parameterized models and the code itself, some quantities were selected and calculated by both the code and NJOY.

Since the topic of the thesis is about the scattering law, it is necessary to see how

the $S(\alpha, \beta)$ behaves compared with the reference, i.e. ENDF-VII. The scattering law could directly indicate if the code works well and the spectra model is reasonable since one could notice the one-to-one correspondence between the $S(\alpha, \beta)$ and the phonon spectrum.

One might be interested in checking the cross sections. They seems more obvious and easier than the scattering law for us to compare with the reference. The THERMR module in NJOY can generate differential inelastic scattering cross sections, $\sigma(E' \rightarrow E)$. Both the Zr and H cross sections were then investigated.

We also checked the average cosine of the scattering angle, $\bar{\mu}$, which is a measure of anisotropy of scattering. Since the $\bar{\mu}$ is calculated with the weighting function of $\sigma(E', \, \mathbf{\Omega}' \cdot \mathbf{\Omega})$, i.e. $\bar{\mu}$ depends on $\sigma(E', \, \mathbf{\Omega}' \cdot \mathbf{\Omega})$, as illustrated in Eq. 2.19, it became a testing case for the scattering cross section.

Continuos energy cross sections are comparable with the reference. A natural question, thereafter, is how about multigroup cross section? The set of parameters given at the beginning of this chapter was used to take the comparisons. Moreover, the cross sections of the ZrH_x, in NSC reactor at TAMU, were calculated with parameters sampled in an LHS design and the ENDF data.

3.2.2   Results and Discussions

$S(\alpha, \, \beta)$, the scattering law

The tabulated scattering laws for some specific α are compared in Figure 3.1 for H in ZrH_x. The results between the parameterized model and ENDF model are comparable. Note that the "symmetric" in the figure labels means $S(\alpha, \beta)$ is symmetric about α axis on the α-β plane.
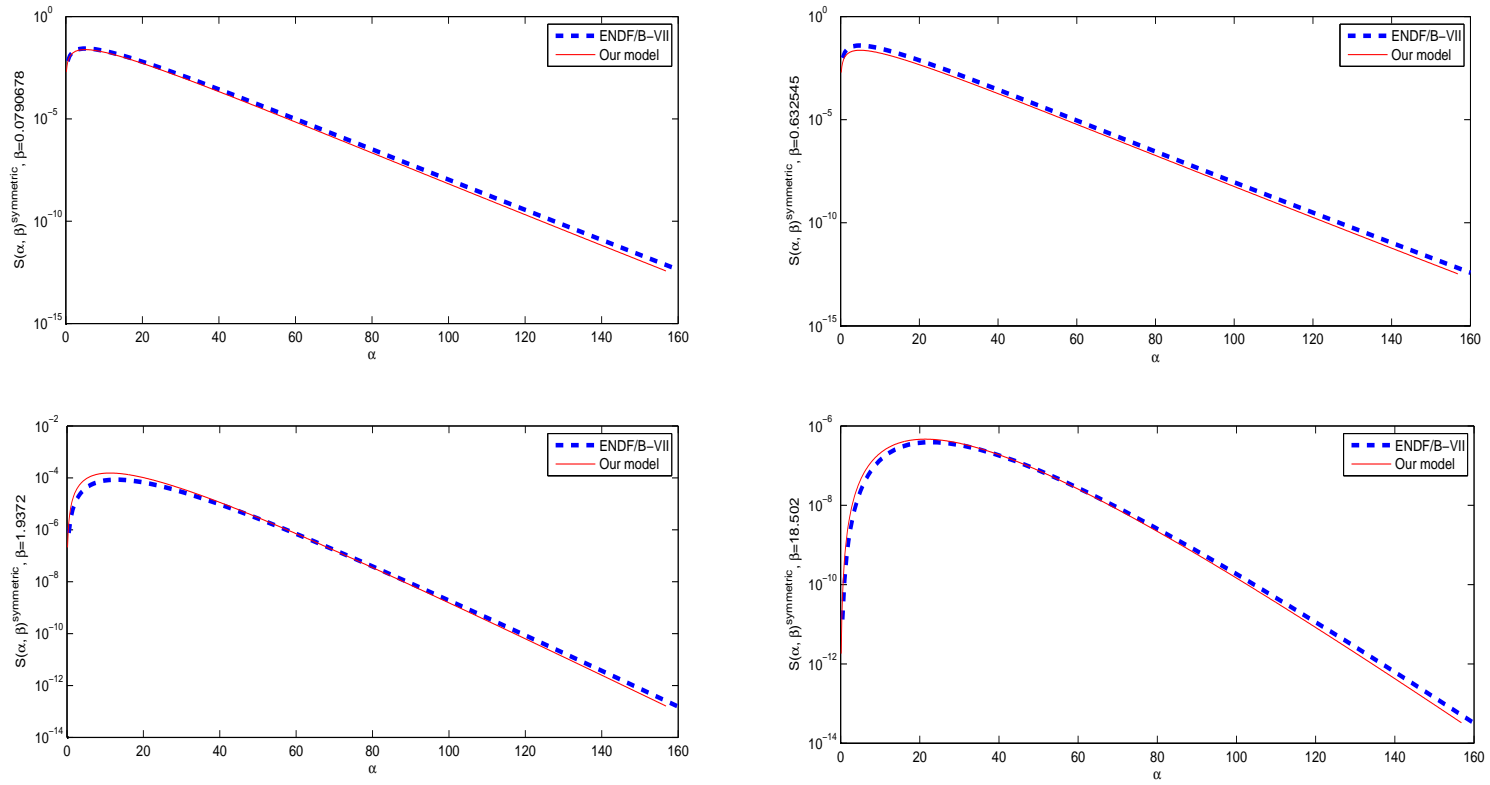
Figure 3.1: $S(\alpha, \beta)$ for specific β for H in ZrH$_x$

For Zr, the scattering laws are shown in Figure 3.2. The laws are also comparable when β is not very large, while they have several orders of differences when β increases.

However, we observe that $S(\alpha, \beta)$ of Zr in ZrH_x is almost negligible, where large difference appears between the reference and the code results, compared with $S(\alpha, \beta)$ of H with the same (α, β). The scattering law is weighted by the bound cross sections, σ_b, of Zr and H in ZrH_x the σ_b^H is more than 10 times larger than σ_b^{Zr}, thus the difference would not cause noticeable errors if we combine the scattering laws to formulate the law for molecule ZrH_x as shown in Eq. 3.3:

$$S(\alpha, \beta)^{\text{ZrH}_x} = \frac{\sigma_b^{Zr}}{\sigma_b^{\text{ZrH}_x}} S(\alpha, \beta)^{Zr} + \frac{x\sigma_b^H}{\sigma_b^{\text{ZrH}_x}} S(\alpha, \beta)^H, \tag{3.1}$$

where the $\sigma_b^{\text{ZrH}_x}$ is given by:

$$\sigma_b^{\text{ZrH}_x} = \sigma_b^{Zr} + x\sigma_b^H. \tag{3.2}$$

For H-1, σ_b^H is around 80 b, while σ_b^{Zr} is around 6.5 b. Take an example for ZrH ($x = 1$), the combined scattering law for the molecule is:

$$S(\alpha, \beta)^{\text{ZrH}} = 0.075 S(\alpha, \beta)^{Zr} + 0.925 S(\alpha, \beta)^H, \tag{3.3}$$

where the weight for H law is more than 0.9. Moreover, with the increase of the H ratio, the weight of H will increase accordingly until 0.96 for ZrH_2. Thus the Zr law would not bring much error for the combined scattering law and equivalently the molecular scattering cross sections.
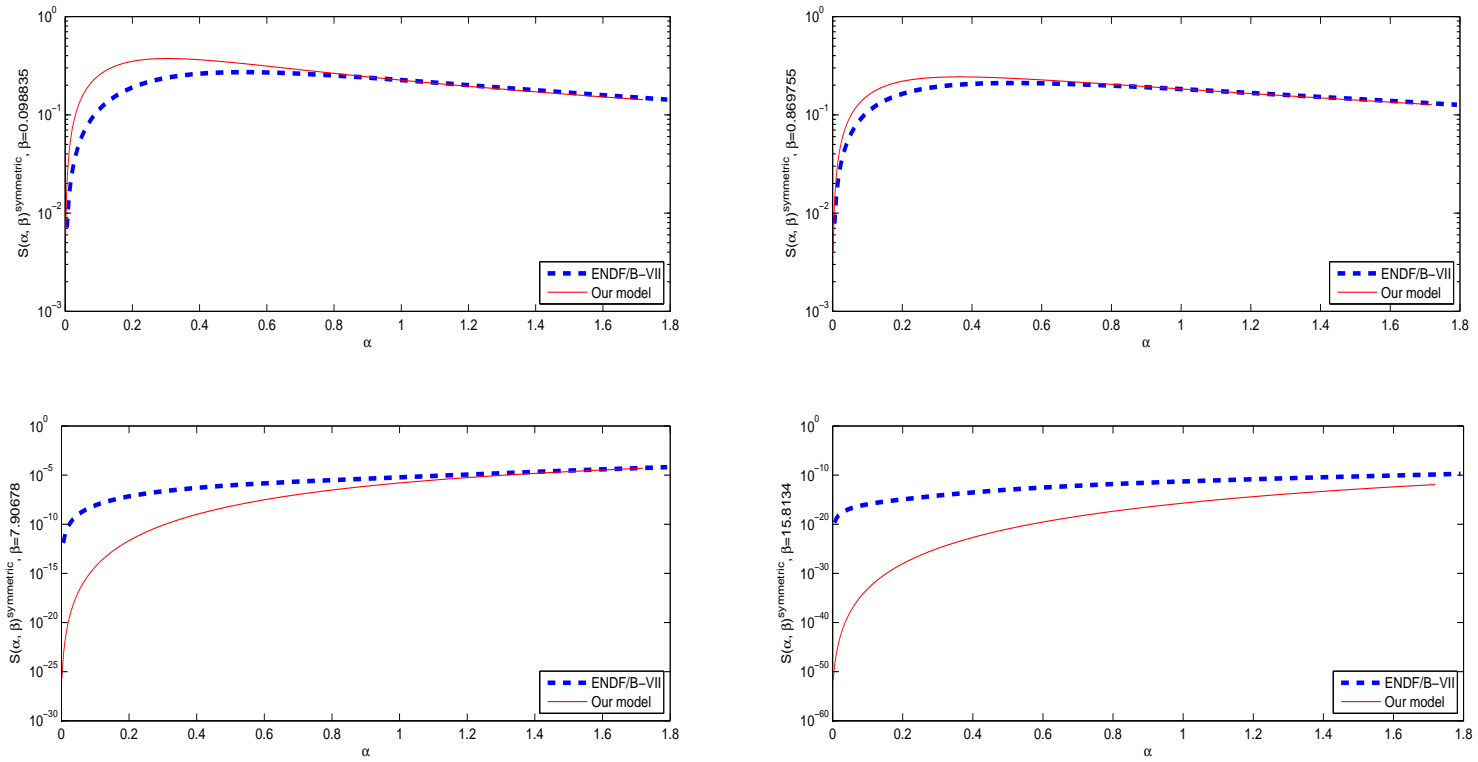
Figure 3.2: $S(\alpha, \beta)$ for specific β for Zr in ZrH_x

The $\sigma(E' \to E)$ with incident energy values of 10^{-5}, $0.62493\,\text{eV}$ and $0.9507\,\text{eV}$ for H and Zr are shown in Figure 3.3. and Figure 3.4, respectively. The selected energy points stand for extremely small energy[1], median energy and large energy, respectively. Note that for median and large incident energy, the code with our model presents similar results with NJOY for both H and Zr. Some differences still occur to the "main peaks" referred to peaks with largest magnitudes. The code gives smooth cross section curves while curves from NJOY are serrated around the main peaks. There are some subpeaks around $137\,\text{meV}$ in CF model while our parameterized models are composed of smooth curves. This may explain this difference of smoothness. Another difference is the "phase-shifting". Though the curves have similar shapes, the peak positions are different. Actually, the shifting could be offset by adjusting the optical peak position to $138.5\,\text{meV}$.

For the very small incident energy, $10^{-5}\,\text{eV}$, however, the parameterized model results differ much from the ENDF results. Observations are the large magnitude difference of the first peak for H as illustrated in Figure 3.3 and the absence of the peak around $0.03\,\text{eV}$ for Zr as shown in Figure 3.4. For the H case, the first peak is the main peak accounted by the optical phonon. We simplified the optical part to a single Gaussian distribution with skipping the fine structures in CF model. This might explain this difference. For the Zr case, we ignored the optical phonon of Zr in ZrH_x for simplicity. Slaggie even proposed a Debye distribution with the peak locating at 20 meV. This simplification totally abandon the details for spectrum beyond the Debye temperature and results show that this simplification would not cause noticable errors [12].

---

[1] 10^{-5} eV is the lower bound of the thermal range in this thesis.
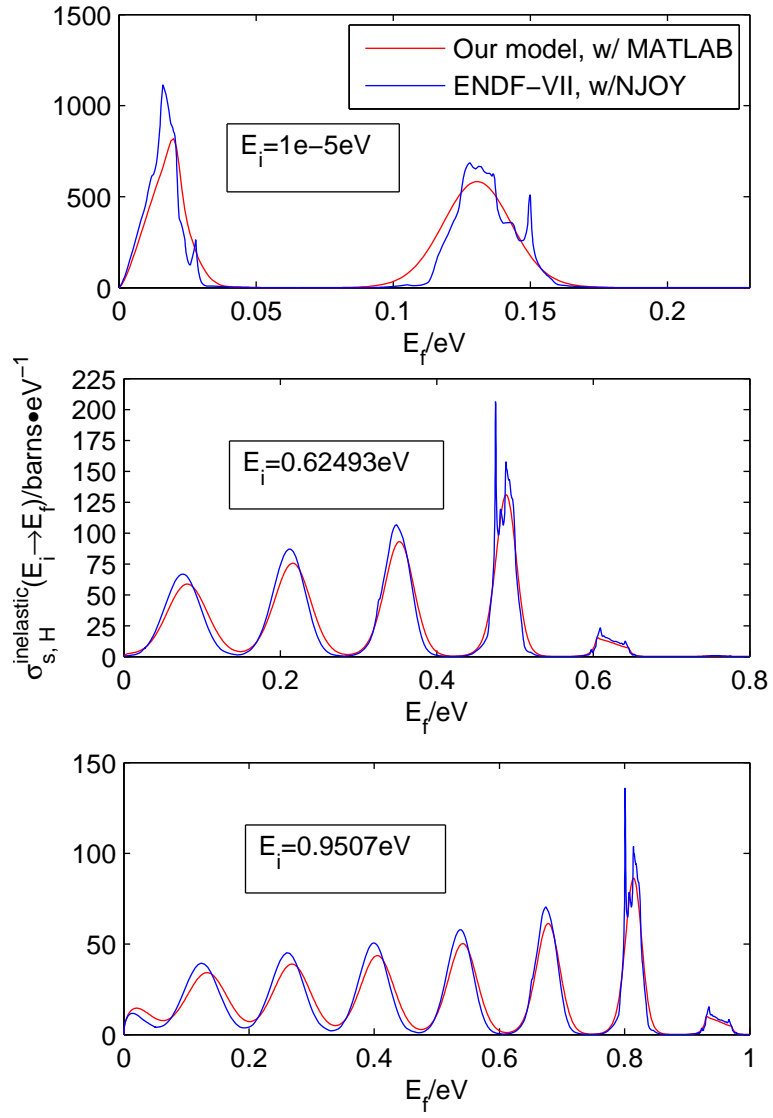
Figure 3.3: $\sigma(E' \rightarrow E)$ for H in ZrH_x.
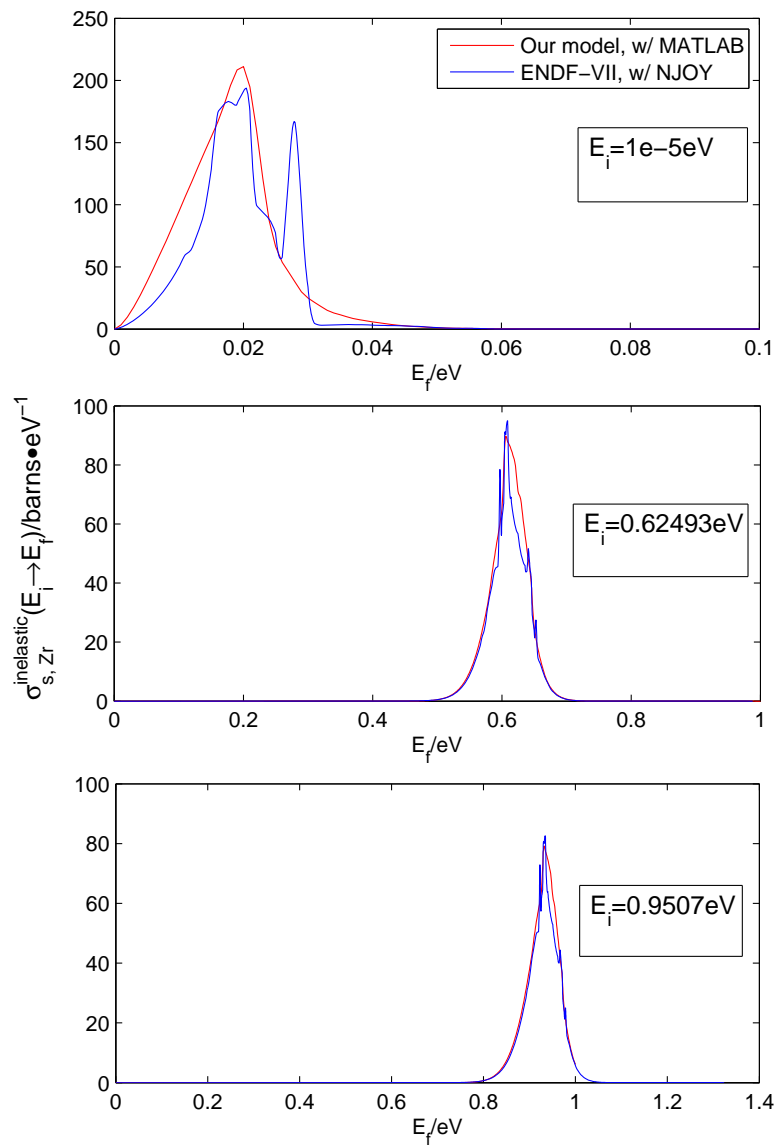
Figure 3.4: $\sigma(E' \to E)$ for Zr in ZrH_x.

$\bar{\mu}$ is calculated with the weighting function of the scattering cross sections, as illustrated by Eq. 2.19. Therefore, the $\bar{\mu}$ should be a good indicator of the weighting functions, $\sigma(E', \mathbf{\Omega}' \cdot \mathbf{\Omega})$. If the weighting function is not close to the reference results, i.e. ENDF-VII, the $\bar{\mu}$ should not be similar with what NJOY presents with CF model.

An example of $ZrH_{1.84}$ was taken referred to the testing cases used by Mattes [8]. Both the cases without and with elastic scattering cross section were investigated as illustrated in Figure 3.5 and Figure 3.6, respectively. The dots in the figures stand for ENDF data processed by NJOY. Good agreement is shown the parameterized model processed by our code and ENDF data processed by NJOY.
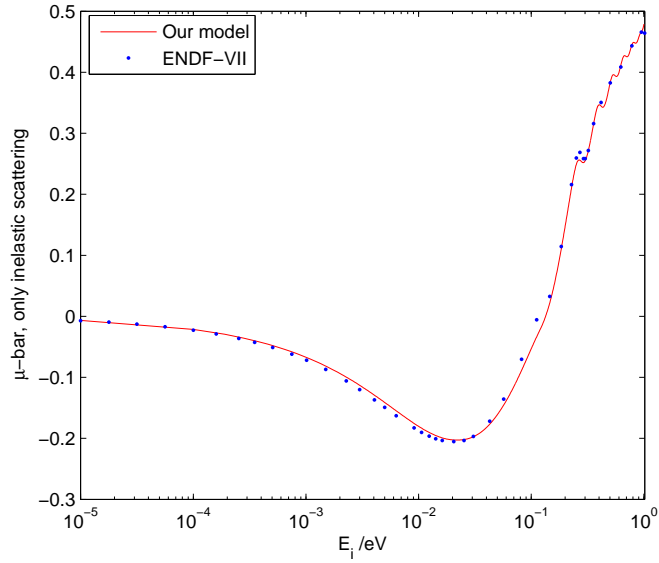
Figure 3.5: $\bar{\mu}$ for $ZrH_{1.84}$, weighted with the inelastic scattering only
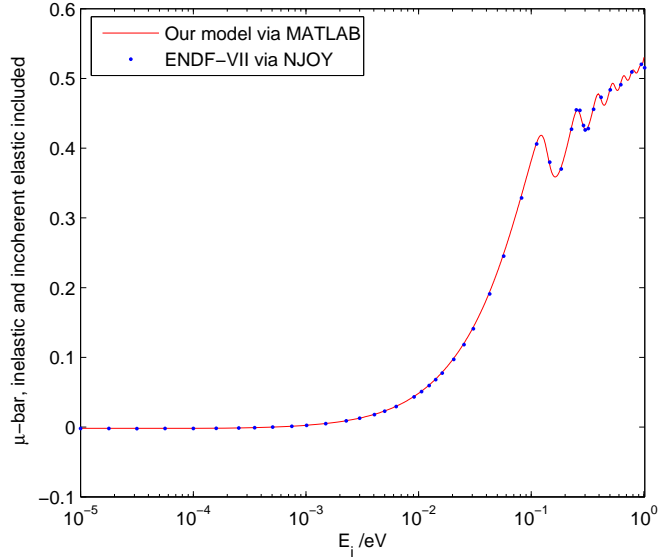
Figure 3.6: $\bar{\mu}$ for $ZrH_{1.84}$, weighted with both the inelastic and elastic scattering

Multigroup Legendre moments of thermal scattering

One purpose of implementing group collapse is such that deterministic transport codes could use it with suitable formats. Via comparing the multigroup constants calculated from the code with the references, on one hand, one could know if the parameterized phonon spectra work; on the other hand, one can know if the integrals involved in the group collapse are correctly done.

The group structure is listed in Table 3.1. For energy lower than $1.13\,\text{eV}$, the Maxwell distribution shown in Eq. 2.22; beyond this energy, the weighting function changes to the $1/E$ spectrum.

Table 3.1: Thermal group stucture used in multigroup constants processing, with forward ordering. The lower boundary of Group 1 is 10^{-5} eV

Group No.	1	2	3	4
Group upper boundaries (eV)	0.0071453	0.029299	0.047302	0.089797
Group No.	5	6	7	8
Group upper boundaries (eV)	0.20961	0.30501	0.39	0.72
Group No.	9	10	11	12
Group upper boundaries (eV)	1.13	1.293	1.6689	2.884

Figure 3.7 and Figure 3.8 are the comparisons for group constants. The results of H from the parameterized model is almost the same as ENDF-VII, while the differences for the Zr constants are noticeble, but they are still within 10%.

Figure 3.9 shows the $ZrH_{1.5229}$, referred to the composition of ZrH_x of NSC reactor at TAMU [10]. We did an LHS design for sampling the parameters within the ranges described previously. The number of the parameter sets are 3000. The numbers in the legend in Figure 3.9 are the number of ordering of the parameter sets. And the multiple lines are generated with parameter sets listed in the legend. One can observe that the data from the parameterized model data vary around the reference. This demonstrates the validity of the parameterized models.
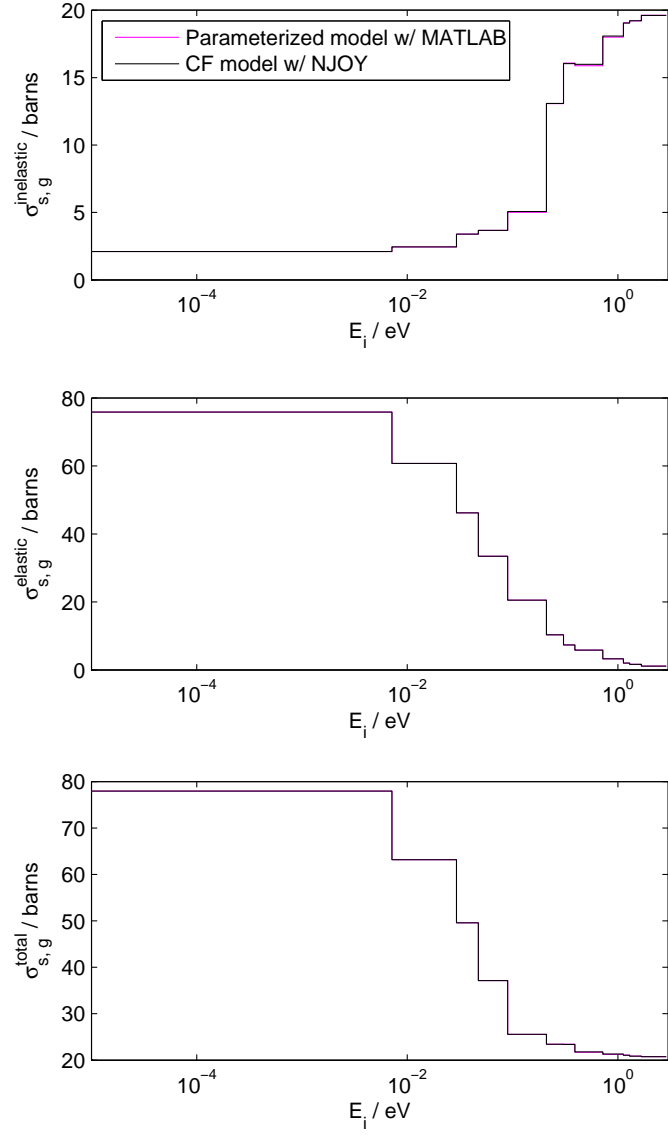
Figure 3.7: Multigroup thermal scattering constants for H in ZrH_x.
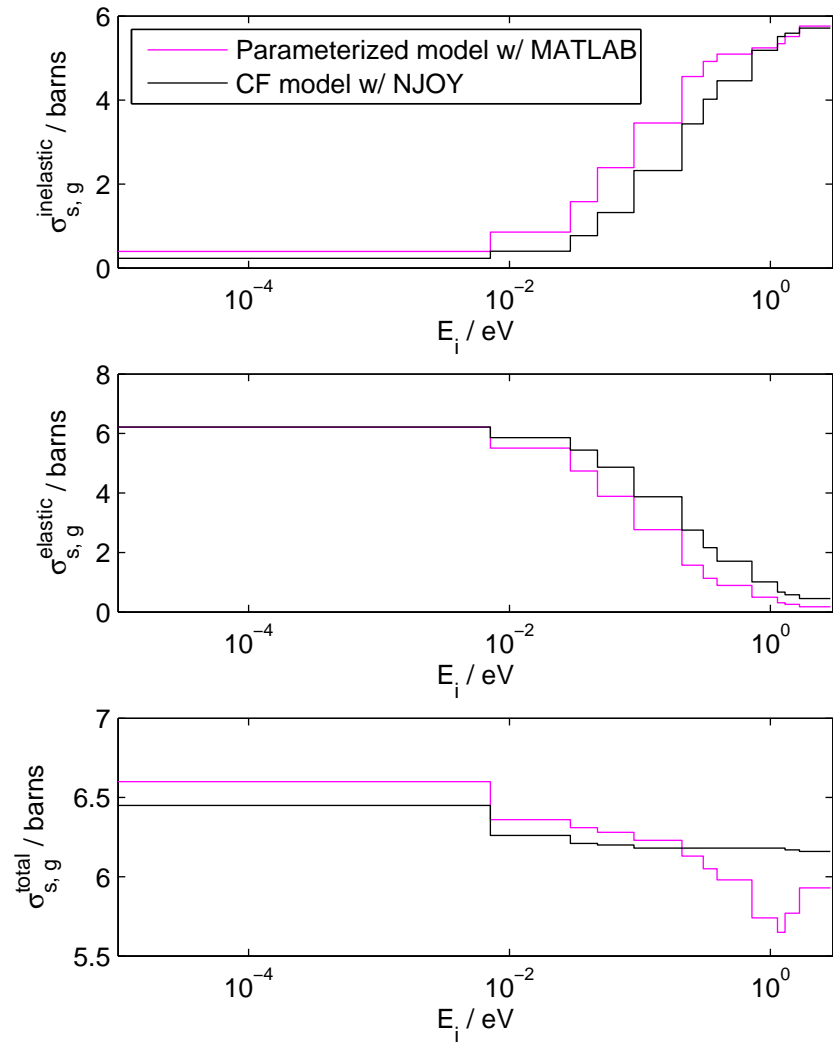
Figure 3.8: Multigroup thermal scattering constants for Zr in ZrH$_x$.
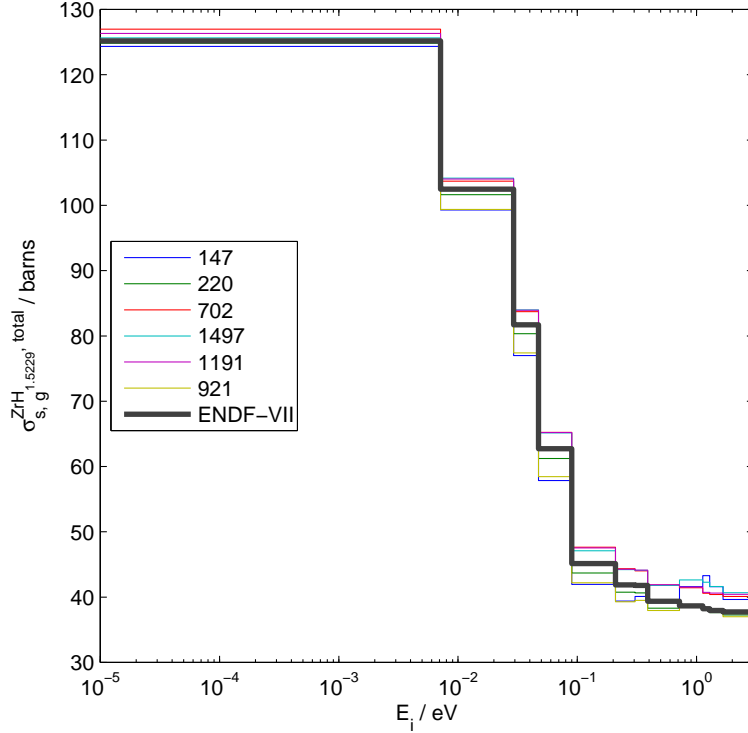
Figure 3.9: Multigroup thermal scattering constants[2] for $ZrH_{1.5229}$

Above all, the multigroup constants match the reference well.

Analytical benchmark for the 0th and 1st Legendre moments of elastic scattering

Fortunately, we are able to find analytical benchmarks in some special cases. With the weighting function of the Maxwell spectrum, as given by Eq. 2.22, and given Debye-Waller coefficient, as illustrated by Eq. 2.16, one would be able to solve for the 0th and 1st Legendre moments of elastic scattering, $\sigma^{\text{iel}}_{0,\,g \to g}$, analytically with equations from Eq. 2.17 through Eq. 2.21.

In this test, we aimed to see the accuracy of the integrators employed to do the group collapse in our code. The Debye-Waller coefficients W, given in Eq. 2.16, of both Zr and H in ZrH (i.e. ZrH_x with $x = 1$),from ENDF-VII were used in the test.

33

The Maxwell spectrum was used as the weighting function for energy lower than 1.13 eV, i.e. Group 1 through 9. And NJOY was involved with the same W as a comparison. Results and corresponding numerical errors for 0th and 1st are listed in Table 3.2 and Table 3.3, respectively.

Table 3.2: Analytical benchmark tests for $\sigma^{\text{iel}}_{0,\, g \to g}$

0th order Legendre moments					
Group No.	Analytic/b	Our code/b	errors / %	NJOY/b	errors / %
1	80.0461	80.0431	0.0037	79.741	0.3812
2	65.4224	65.4126	0.0149	64.6717	1.1475
3	50.8769	50.8704	0.0129	50.331	1.073
4	36.868	36.8472	0.0564	35.3481	4.1227
5	23.1116	23.086	0.1107	20.0264	13.3491
6	12.513	12.507	0.0479	11.57	7.536
7	9.151	9.1487	0.0251	8.7832	4.0196
8	7.5042	7.5074	0.0431	5.7816	22.9553
9	3.8984	3.8983	0.0017	3.5992	7.6759

It can be observed that our code agrees better to the analytical solutions than NJOY does for both the 0th and 1st orders.

Table 3.3: Analytical benchmark tests for $\sigma^{\text{iel}}_{1,\ g \to g}$

1$^{\text{st}}$ order Legendre moments					
Group No.	Analytic/b	Our code/b	errors / %	NJOY/b	errors / %
1	2.6989	2.6997	0.0283	2.7436	1.654
2	6.8087	6.8111	0.0354	6.9598	2.2189
3	10.0231	10.0242	0.0114	10.0898	0.6655
4	11.6673	11.6683	0.0089	11.7201	0.4531
5	11.1728	11.1682	0.0408	10.5212	5.832
6	8.2819	8.2793	0.0304	7.8643	5.0422
7	6.6869	6.6857	0.0177	6.4935	2.8929
8	5.7721	5.775	0.0511	4.688	18.7813
9	3.3994	3.3995	0.0014	3.1723	6.6813

IV. SIMULATIONS AND ANALYSES FOR SINGLE LATTICE

We chose the NJOY-MCNP chain for the UQ study. Though MCNP can be time-consuming and suffer from slow convergence and computational expensiveness, it has been demonstrated to model neutron transport accurately and realistically. Additionally, NJOY is able to process MCNP-compatible scattering cross sections, given phonon spectra, for both Zr and H within minutes.

The objective of the thesis is to quantify the uncertainties of the QOIs in TRIGA reactor simulations due to the uncertainty of the phonon spectra of the ZrH_x characterized by seven parameters. Before simulating the full-core TRIGA model, a single lattice model was investigated. The single lattice simulation has the advantage of structural simplicity and relatively short time per simulation. The purpose of simulating the single lattice model in this thesis are as follows

1. Test the feasibility of the methods as planned for this UQ study.

2. Find possible QOIs sensitive to the variation of the phonon spectra.

3. Determine which parameters these QOIs are sensitive to.

Techniques involved in the analysis part are LHS, ANOVA and regression. LHS samples parameters uniformly in corresponding intervals of parameters; the ANOVA is able to give the relative importance of factors to the QOIs; according to the ANOVA results, important factors are engaged in the regressions. The input parameters for the regressions are in standardized forms such that the absolute values of the coefficients also indicate the importance of parameters as the ANOVA does, i.e. it provides the comparability of different parameters on a dimensionless scale.

The reactivity, ρ and the fission rate density, FRD, were selected as QOIs in the lattice model simulations. It is reasonable to hypothesize these two quantities are sensitive to the phonon spectrum variations. Since the phonon spectrum variations induce the variation of the thermal scattering cross section, as shown in Figure 3.9, the moderation, upscattering, etc. would change, which would affect and reactivity and the FRD.

4.1 Calculation Flow and Simulation Model Description

4.1.1 Calculation Flow

The calculation process shown in Table 4.1 involves several modules of NJOY: LEAPR, RECONR, BROADR, THERMR and ACER. If we skip the intermediate steps, the process is like a black-box process: given input, output QOIs. And the flow table is exactly the same for the full-core case except the different MCNP decks.

Table 4.1: Calculations flow

Step No.	Codes/techniques and corresponding work
1.	Sample the parameters by the LHS technique;
2.	Generate the parameterized phonon spectra with the sampled parameter sets;
3.	Invoke the LEAPR module of NJOY to tabulate the scattering law;
4.	Invoke the RECONR and BROADR modules of NJOY to prepare the Pointwise ENDF data (PENDF);
5.	Invoke the THERMR module of NJOY to process thermal scattering cross sections;
6.	Invoke the ACER module of NJOY to transfer the data to the MCNP-compatible ACE format; reinvoke ACER to check the fatal errors, such as nagative probability;
7.	Run MCNP with thermal treatment using the data generated in Step 6;
8.	Extract and process the QOIs and do the analyses.

4.1.2 Lattice Model Description

The MCNP deck for single lattice of TRIGA reactor was built. On the top of the fuel pin, there is the moderator, light water, with a depth of 110.95cm. Instead of full-pin model, the 1/16-lattice model was used as illustrated in Figure 4.1. The three vertical surfaces and the axial cross section are set to be reflective such that the model is actually an semi-infinite model.
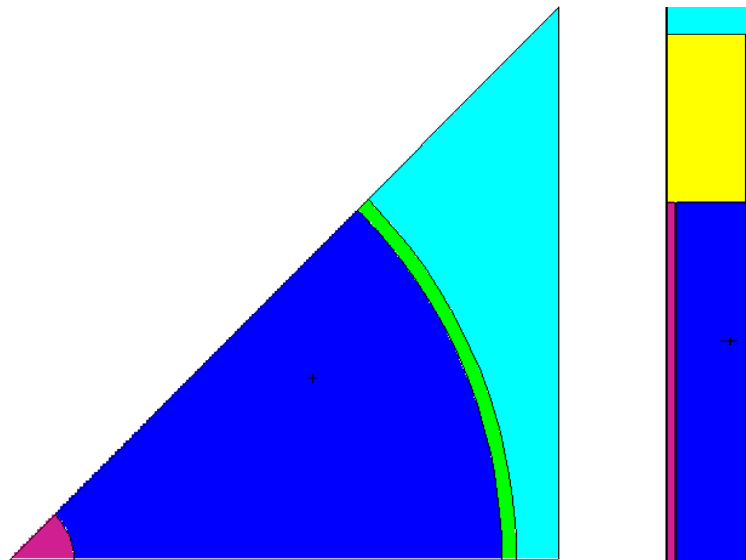
Figure 4.1: TRIGA lattice model

The fuel material is U-ZrH$_x$ with the x of 1.5229 and U-235 enrichment of 19.75 [10]. The central part of the fuel rod is made of zirconium. The axial reflector is made of graphite.

In the control cards of the MCNP deck, the kcode card is filled as:

```
kcode 50000 1 30 260
```

50000 means the total number of neutrons tracked in a cycle is 50000; 1 is the initial guess for k_{eff}; 30 is the number of cycles which are ignored at the beginning; 260 is the total number of cycles run in the criticality calculations. Thus, there are 1.3×10^7 neutrons in total, which lead to the standard deviations of k_{eff} around $21\,\mathrm{pcm}$[1] for each simulation.

The LHS design function in MATLAB (Function lhsdesign) was induced to generate 3000 sets of parameters, within the ranges discussed previously, to produce correponding parameterized phonon spectra for H and Zr ZrH_x. No option was specified for the MATLAB function. We determined to choose the sample size of 3000 is because we expected a large size of the simulations to make the statistical models based on the simulation results more accurate and simultaneously these simulations could be done in limited time.

4.2   Results, Observations and Analyses

4.2.1   Standardized Parameters

Denote FWHM, b, p, T_{DH}, T_{DZr}, r and c by P_1 through P_7, respectively. And the means and standard deviations for corresponding parameters generated in LHS process by μ_i and σ_i ($i = 1, \cdots, 7$). And denote the standardized forms of P_i by X_i, $i = 1, \cdots, 7$. Then the standardized parameters can be given by

$$X_i = \frac{P_i - \mu_i}{\sigma_i}. \tag{4.1}$$

4.2.2   N-way ANOVA

ANOVA is the abbreviation of "Analysis of Variance", which is a collection of statistical tests for heterogeneity of means of experiment outcomes by analysis of

---

[1] $1\,\mathrm{pcm} = 1 \times 10^{-5}$.

group variance [14]. It attempts to analyzes the variations of the responses to each variable in a set of independent variables [13]. Through the ANOVA procedure, one would archive information such as: degree of freedom of each variable (DF), sum of squares (SS), mean squares, F-test statistic and p-value. [5] The objective is to use the information above to identify the important variables and corresponding effects to the responses [13].

N-way ANOVA is the ANOVA for testing the effects of multiple factors on the mean of the experiment outcomes [15]. In the outcome of n-way anova, one could discriminate the important factors (may include interactions) from unimportant ones[11]. The ANOVA tables for ρ and FRD in this chapter are given and put in Appendix A. The criteria choosing the principal factors, including interactions and high order terms are based on the ANOVA table. The MeanSq is the mean sum of squares (MS). It measures the importance of the factors to the experiment outcomes[11]. And the F value is the ratio of explainable variances (theory) to unexplainable variance (error). It tells if the factors and the QOIs are correlated. And p-value is also an important criteria especially when the mean squared sum (MSS) do not dominate over the mean squared errors (MSE) much. In this thesis, we rejected the null-hypothesis with p-value of 0.05. The ANOVA tables in Appendix A show that X_2 (standardized branching ration, b, of the acoustic phonon for H in ZrH_x) and X_3 (the standardized peak position, p, of the optical phonon for H in ZrH_x) might be the most important two parameters for QOIs in this chapter.

4.2.3 Cross Validations with Regressions

Based on our findings from ANOVA, we built regression models and then performed cross validations to confirm the validity of the models. In corss-validations, we separate the set of input samples and their corresponding outputs into a training

and a test sets. The training set is used to create regression models, and then using these models we predict outputs for the test set. Using the error between the outputs predicted from the model and the actual outputs in the test set, we can select models based on accuracy and parsimony.

We trained the data for both reactivity and FRD. And there is the test part corresponding to the training part. In this thesis, the ratios of the numbers of samples in the training sets to the test sets in cross-validations are set to be 0.8. Therefore, for the study based on the TRIGA lattice geometry, there are 2400 cases for the training set and 600 cases for the test set.

One fact is that ANOVA though indicates the significance of each factor, including interactive terms and high order terms, may not truly reveal whether the QOIs are sensitive to the factors. This is the reason that we made the cross validations follow the ANOVA. We aimed to test the sensitivities of QOIs indicated by ANOVA via using cross validations.

Basically, those QOIs, e.g. reactivity, Λ (which will be introduced in the next chapter), etc., which pass the sensitivity tests with cross validations, will be designated to calibrate the proposed parameters, especially to calibrate the principal parameters
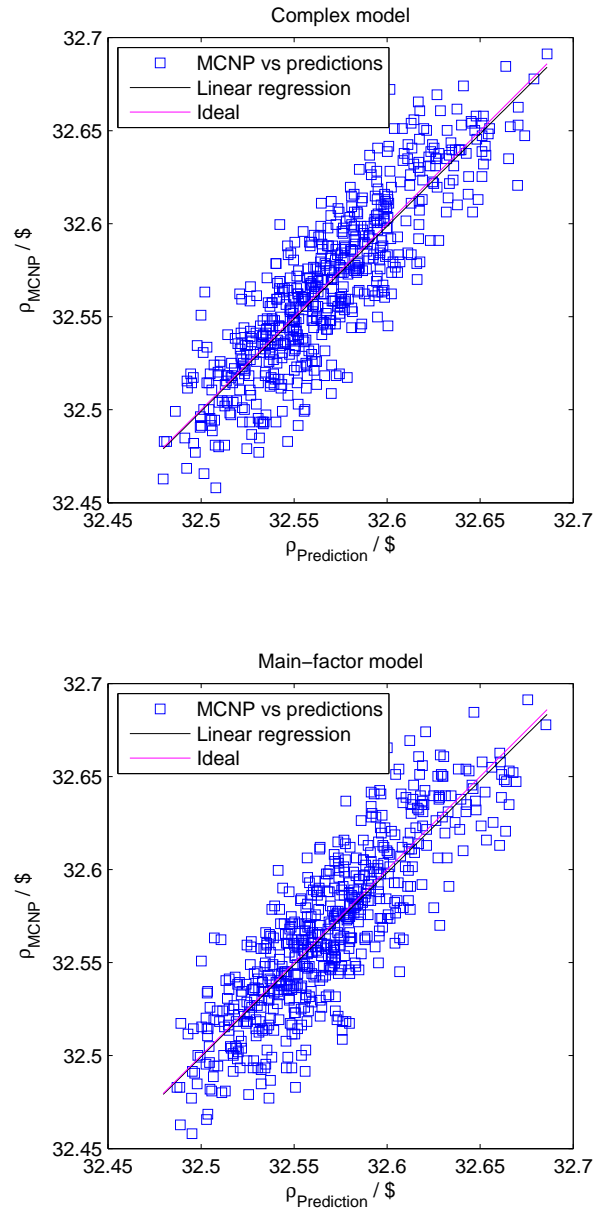
Figure 4.2: Cross validations for ρ

For ρ , the testing plot are shown in Figure 4.2. The upper figure regressed with

all the the significant factors indicated by the ANOVA table Table A.1. The lower plot regressed with only the factors containing X_2 and X_3. The regression coefficients are listed in Tables in Appendix A. For the simple model, which we called main-factor model (recall that X_2 (standardized branching ratio of H acoustic phonon) and X_3 (standardized H optical phonon peak position) are the main factors in this thesis.). The main-factor model is shown in Eq. 4.2.

$$\rho = 32.564 + 2.5339 \times 10^{-2} X_2 - 2.1105 \times 10^{-2} X_3$$
$$- 1.8799 \times 10^{-3} X_2 X_3 + 5.2404 \times 10^{-3} X_3^2 - 4.3131 \times 10^{-3} X_3^2 \tag{4.2}$$

The R^2 is 0.687. The regression coefficients have different magnitudes. One might find that the factors having coefficients with larger magnitudes in the regression also have higher significance indicated in ANOVA tables. Actually, this observation demonstrates that regressions for standardized factors is an alternative effective way to determine the importance of factors [11].

For FRD, the testing plot is shown in Figure 4.3. The important factors indicated by Table A.5 are only X_2 and X_3, which are also the main factors. The main-factor model is given by

$$\text{FRD} = 4.2117 + 4.2499 \times 10^{-4} X_2 - 4.4680 \times 10^{-4}. \tag{4.3}$$

The R^2 is 0.0944.
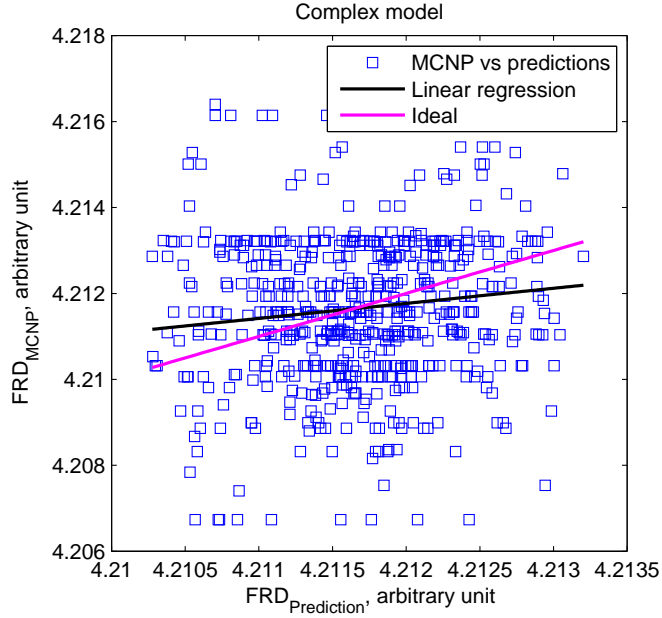
Figure 4.3: Cross validations for FRD

4.2.4 Comparisons of Parameterized Spectra with IKE and ENDF Models

Chapter 3 presents some comparisons between the phonon spectra hypothesized in this thesis and other published results. The results show the hypothesis for the parameterized models are reasonable. Ultimately, we would like to compare our model to published models on real QOIs.

The parameterized spectra are expected to give results close to the references for some values of the parameters. In other words, we expect the reference results will be surrounded by QOIs from the parameterized models within the ρ-FRD plane.

QOIs are ρ and FRD for the lattice model. Scatterplots for QOIs from the parameterized models postulated in this thesis and the references, i.e. IKE with the DG and ENDF with the CF models, are shown in Figure 4.4. The reference points

45

are within the QOIs from our models. This lends support to the parameterized phonon spectrum models.
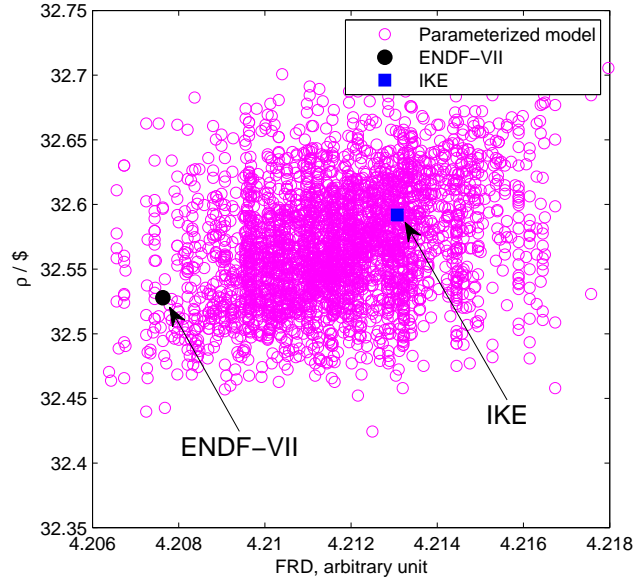
Figure 4.4: Scatterplots on the QOI plane

One would have observed that the locations of the two references are different. The scatterplot indicate distinct ρ and FRD for them. Since different points are generated with different sets of parameters, this might indicate that if one want to archive similar results to the two references with the parameterized models, ethe parameter choices must be different.

4.2.5 Score Estimation and Parameter Dependency

We developed the parameterized models and we aim to calibrate proper parameter sets for the TRIGA reactor at TAMU. For the calibration, we "score" how close a particular QOI is to the target or reference QOI.

46

Results from MCNP simulations are given in distribution forms: mean values with standard deviations. Thus we defined the score to refer to the overlapped area between the QOI distributions from the parameterized models and the reference results. These reference results are the examples of calibrations. These references play the role of experimental results. The aim is to test the feasibility of implementing calibrations once we have some experimental QOIs.

And the derivation for the calculation of the score is attached in Appendix C. The original expectation was that the high scores distribute in some specific regions in the seven dimensional parameter space. And the preference of the parameter ranges are the calibrated results for specific QOIs. Once several calibrations for different sensitive QOIs are done, the high score region is expected to narrow down.

Based on cross validation results, the branching ratio of acoustic mode to optical mode in H and optical peak position in H spectrum are the most important two factors. We then plotted the score for each QOI on the main-factor plane, i.e. the X_2-X_3 plane (X_2 and X_3 are the standardized forms of the two factors mentioned above, respectively.), such that the "spatial" distributions would indicate what the dependencies of each QOI on the main factors are, as shown in Figure 4.5 and Figure 4.6.
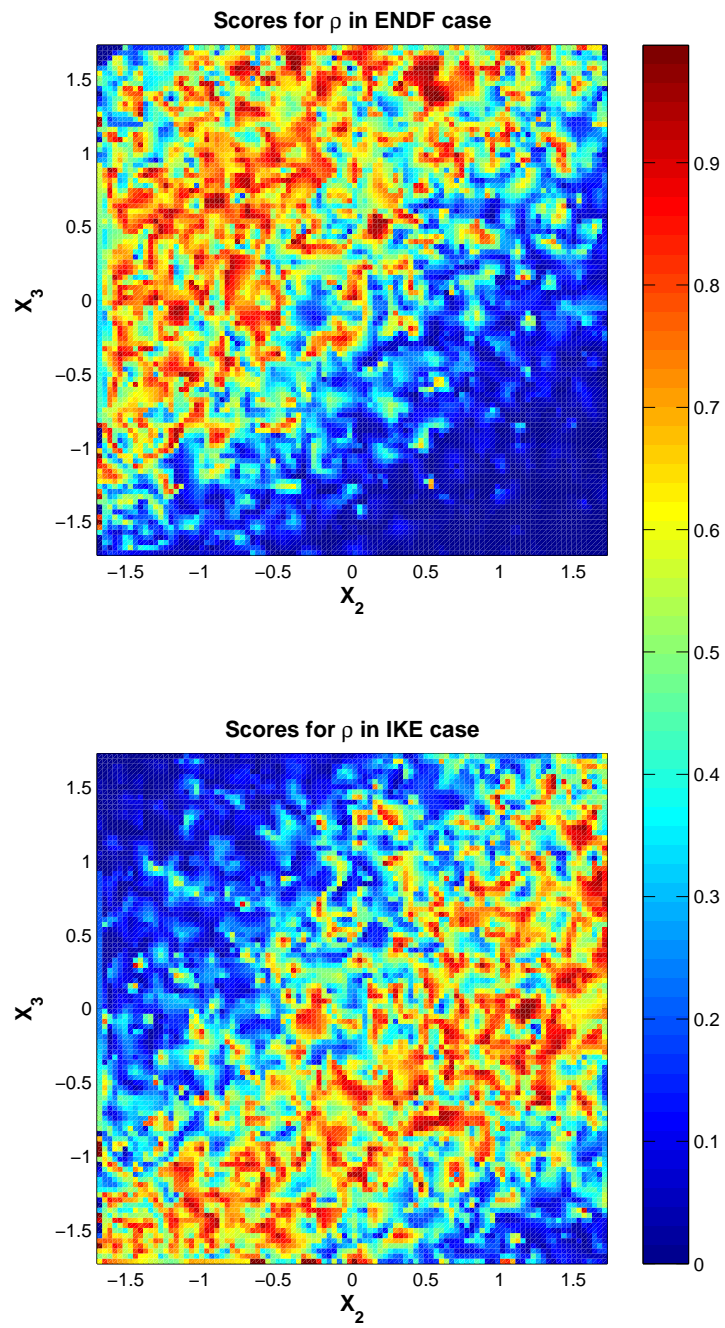
Figure 4.5: Score distributions for ρ on main-factor plane

One may have noticed that, for ρ, the scores in the two reference cases have different distributions on the main-factor plane, which is somewhat consistent with the situation shown in Figure 4.4. And it also reflects the sensitivity of ρ to the main factors: reactivity varies when main factors vary.

Another observation is that for scores of ρ in different cases, the high score regions forms bands within different different ranges of the main factors. This would indicate for specific QOIs, the scores for the references, e.g. QOIs from experiments, could be specify if the QOI investigated is sensitive to the parameters. More importantly, if several different QOIs are sensitive to the parameters, the overlapped high score regions for different QOIs would be very fine such that one might be able to specify the choice of parameters to generate parameterized phonon spectra, or equivalently the scattering laws, which make the reactor simulation results close to the reference(s). If the reference is accurate, the parameterized models would be close to the realistic ones. This is also known as calibration mentioned in previous sections, where one uses measured QOIs to constrain uncertain parameters.
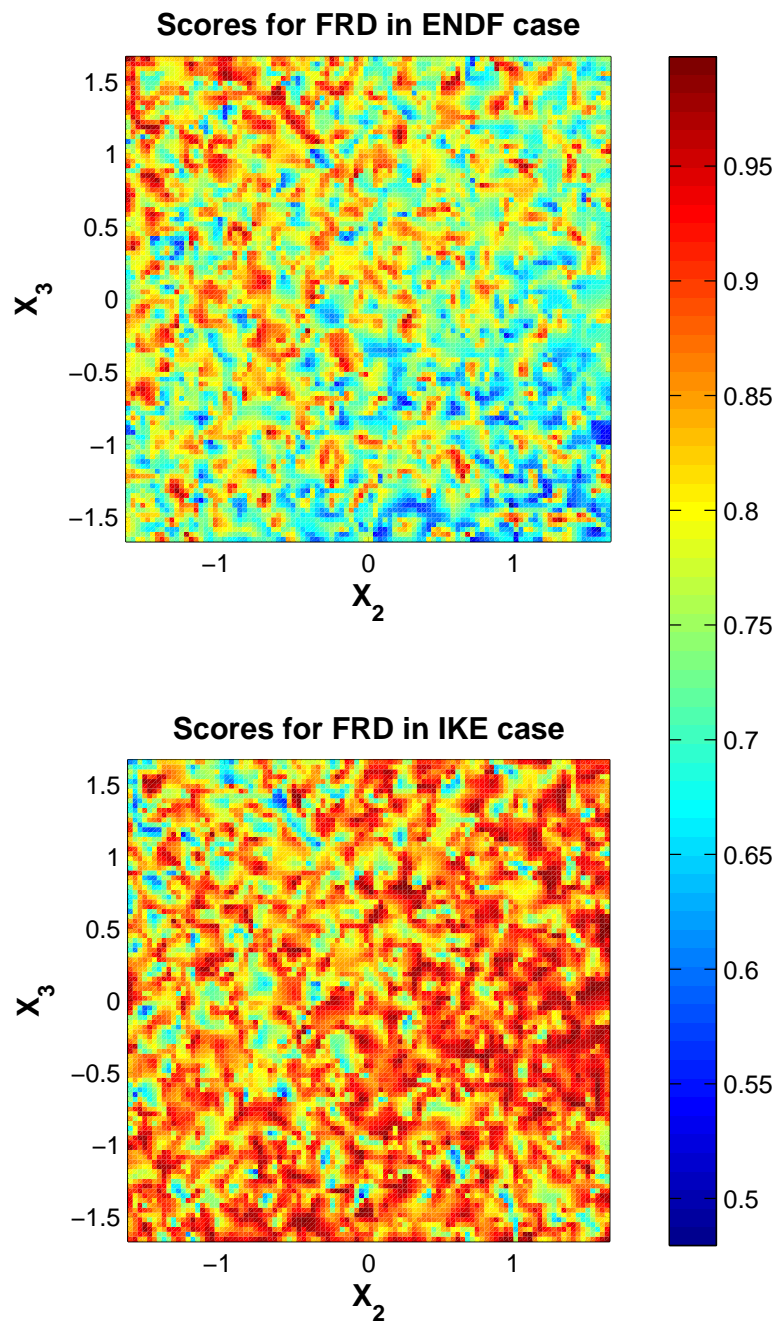
Figure 4.6: Score distributions for FRD on main-factor plane

The scores for FRD in both IKE and ENDF cases indicates the insensitivity of FRD to the main factors. The scores are high everywhere in both cases, which can be interpreted as FRD stays as a constant whatever factor values are. This observation is consistent with what we have noticed from the cross-validations.

4.3 Directions for Full-core Model Analyses

Methods used in this chapter, including ANOVA, cross validation, score estimation reveals the sensitivity of ρ to the parameters. This would indicate the feasibility of the analysis methods in the following full-core analyses. The insensitivity of the FRD implies that some QOIs may not be sensitive to the thermal scattering law, or equivalently, the phonon spectrum.

V. SIMULATIONS AND ANALYSES FOR FULL-CORE TRIGA MODEL

As implied by the results for the lattice model, the ANOVA-cross validation strategy with estimating *score* distributions is effective in this UQ study. In this chapter, these techniques are extended to apply in the full-core model analyses. The calculation flow is still shown in Table 4.1, propagated from the LHS for parameters to data processing and finally to QOIs. Moreover, we considered more QOIs than we used previously. Similar to the lattice-model results, some QOIs show sensitivity while some do not.

An extension of optical phonon peak position of H in ZrH_x p from [132, 142] meV was implemented to the range of [137, 147] meV [12].

Moreover, ex-core detectors were added and the absorption rates were investigated with 100 more MCNP simulations. The results indicate that the absorption rate would not be insensitive to the parameters.

5.1 Simulation Model and QOIs Description

5.1.1 MCNP Settings

The full-core geometry used in our simulations is presented in Figure 5.1 [10]. There are four regular control rods (dark orange), a transient rod (white) and a shim safety rod (light pink). The blue rods are fuel rods. Around the core, there are graphite blocks (yellow) and water (cyan). The position adjustment of the rod is based on the a standard configuration for control rod worth measurement at NSC, TAMU. The configuration for each control rod is such that the reactor stays subcritical. The temperature is set at 300K. The fuel rods are the exactly the same as the one in Chapter 4. In order to archive reasonably small errors, the total number of neutrons was set to be large in the MCNP deck. The kcode card in the control cards is:

52

```
kcode 90000 1 30 500,
```

which means we have 90000 tracked neutrons per cycle with a total cycle of 500, which makes there be 4.5×10^7 neutrons in total per simulation. With this configuration, the standard deviation of k_{eff} reduced to 13 pcm.

In the LHS design, we generated 2100 sets of parameters and produced 2100 data files for each atom in ZrH_x at 300 K and 400 K, respectively (Thus it is 8400 thermal neutron scattering data files in total.). And we then run 6300 MCNP cases in total (2100 were for MCNP decks with delayed neutron accounted at 300 K, 2100 were for decks without delayed neutrons accounted at 300 K and the rest 2100 cases were for decks at 400 K with delayed neutrons accounted.). Unfortunately, about 10% decks failed with misoperations. After all, we archived 1982 cases for ρ and Λ investigations, 1972 cases for β_{eff} investigation and 1216 cases for α_T^{Fuel}.
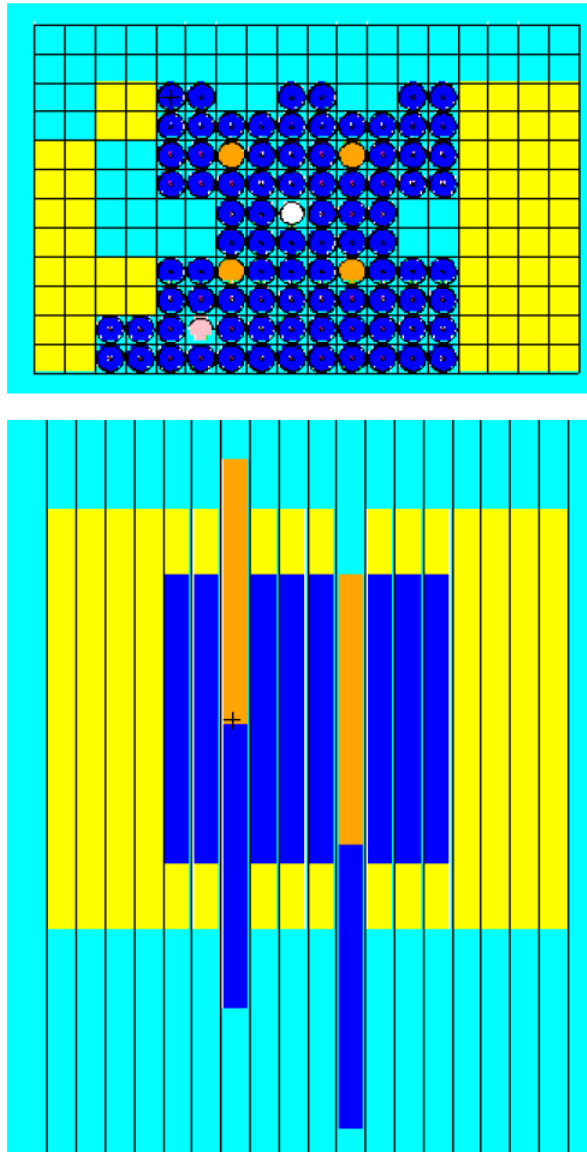
Figure 5.1: Full-core TRIGA Model for MCNP

5.1.2 QOI Descriptions

From the work for lattice model analyses, the sensitivity of the reactivity to the parameters was revealed (Equaivalently, k_{eff} is sensitive.). Therefore, a reasonable hypothesis is that quantities correlated with the reactivity, or k_{eff}, might be sensitive

to the phonon spectra. With this reasoning, reactivity ρ, neutron mean generation time Λ, effective delayed neutron fraction β_{eff} and fuel temperature feedback coefficient were investigated. The expressions for these four QOIs are illustrated from Eq. 5.1 through Eq. 5.4. Note that Eq. 5.8 is the way to obtain the β_{eff} in MCNP.

$$\rho = \frac{k_{\text{eff}} - 1}{k_{\text{eff}}} \tag{5.1}$$

$$\Lambda = \frac{l_p}{k_{\text{eff}}} \tag{5.2}$$

$$\beta_{\text{eff}} = \rho - \rho_{\text{prompt}} \tag{5.3}$$

$$\alpha_T^{\text{Fuel}} = \frac{d\rho}{dT_{\text{Fuel}}} \approx \frac{\rho(T_{\text{Fuel, 1}}) - \rho(T_{\text{Fuel, 2}})}{T_{\text{Fuel, 1}} - T_{\text{Fuel, 2}}} \tag{5.4}$$

Note that the reactivity and β_{eff} is dimensionless.

5.2   Results and Analyses

5.2.1   ANOVA Results and Factor Selections

As a convention in this work, we present and discuss the ANOVA results, as shown in Table B.1, B.5, B.9 and B.13, at the very beginning of the analyses. Those tables present analyses for basic parameters, second order interactions and some high order terms of the main parameters. The same critiria, as declared in Chapter 4, i.e. large MeanSq and F values with p-value smaller than 0.05, were used to determine factor significance.

For ρ, Λ, and α_T^{Fuel}, significant factors were selected and shown in the "Observations" in Table B.3, B.7 and B.14, respectively. For β_{eff}, there might be two important factors, i.e. X_3 and the interaction term $X3 : X7$. However, previous trials for cross validation for β_{eff} with these two terms presents strange and unacceptable results. Therefore only X_3 (the optical phonon peak position of H in ZrH_x) is selected as

55

the important factor for β_{eff}.

5.2.2   Cross Validations

Cross validations were taken for all QOIs with all important parameters. The regression coefficient tables are shown in Appendix B marked as "complex model". The coefficients in each coefficients table show the significance with p-values. Simplifications using terms containing only X_2 (the standardized branching ratio of acoustic phonon of H in ZrH$_x$) and/or X_3, i.e. X_2, X_3, X_2X_3, X_2^2, X_3^2, etc., are made to models of ρ, Λ and α_T^{Fuel} and are marked as "main-factor model".

Cross validations for ρ

For ρ, cross validation results are presented in Figure 5.2 and the main-factor model is shown in Figure 5.2 on Page 57. For both models, the testing parts show good agreement between the predictions and the MCNP simulations. One would notice that the main-factor model probably gives better results in this case. In the coefficient tables in the Appendices, the R^2 are given in the titles. For ρ for the full-core TRIGA model, R^2 are 0.926 and 0.955 for the complex model and main-factor model, respectively.

$$\begin{aligned}
\rho = &- 3.8793 + 3.9815 \times 10^{-2} X_2 - 1.0728 \times 10^{-1} X_3 \\
&+ 2.9019 \times 10^{-2} X_3^2 - 1.8434 \times 10^{-2} X_3^3
\end{aligned} \tag{5.5}$$
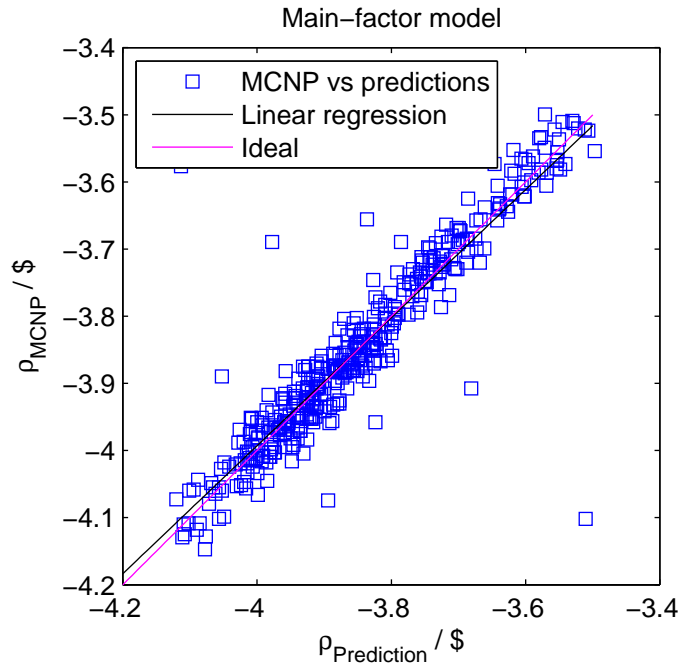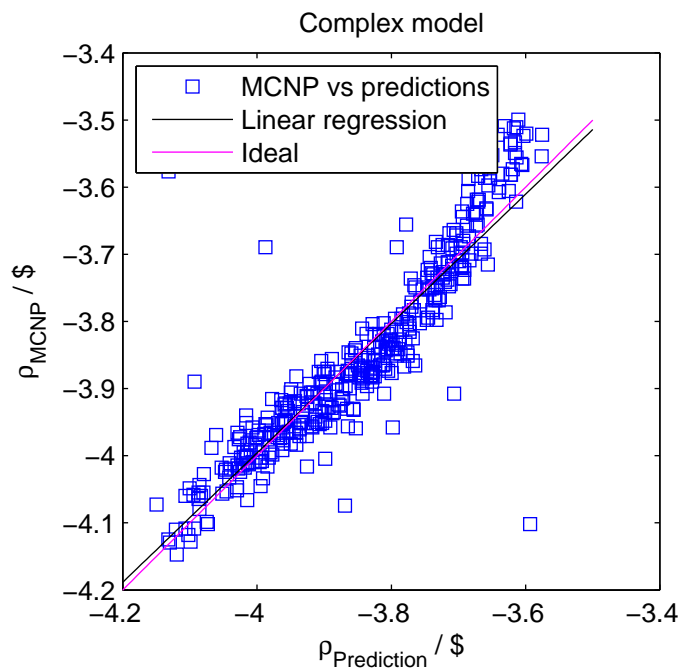
Figure 5.2: Cross validations for ρ

Cross validations for Λ

Since the reactivity shows sensitivity to the parameters, it is also reasonable to expect such results for Λ, also. Both the complex and the main-factor models work well, as shown in Figure 5.3. And the main-factor model is presented in Eq. 5.6. R^2 for the complex model and main-factor model are 0.918 and 0.907, respectively. This might indicate that using main-factor model would not induce such large error. And it would even give better predictions in some special cases.

$$\begin{aligned} \Lambda =&7.8183 \times 10^{-5} - 3.7219 \times 10^{-8}X_2 + 8.7285 \times 10^{-8}X_3 \\ &- 2.7854 \times 10^{-2}X_3^2 + 1.9164 \times 10^{-8}X_3^3 \end{aligned}$$

(5.6)
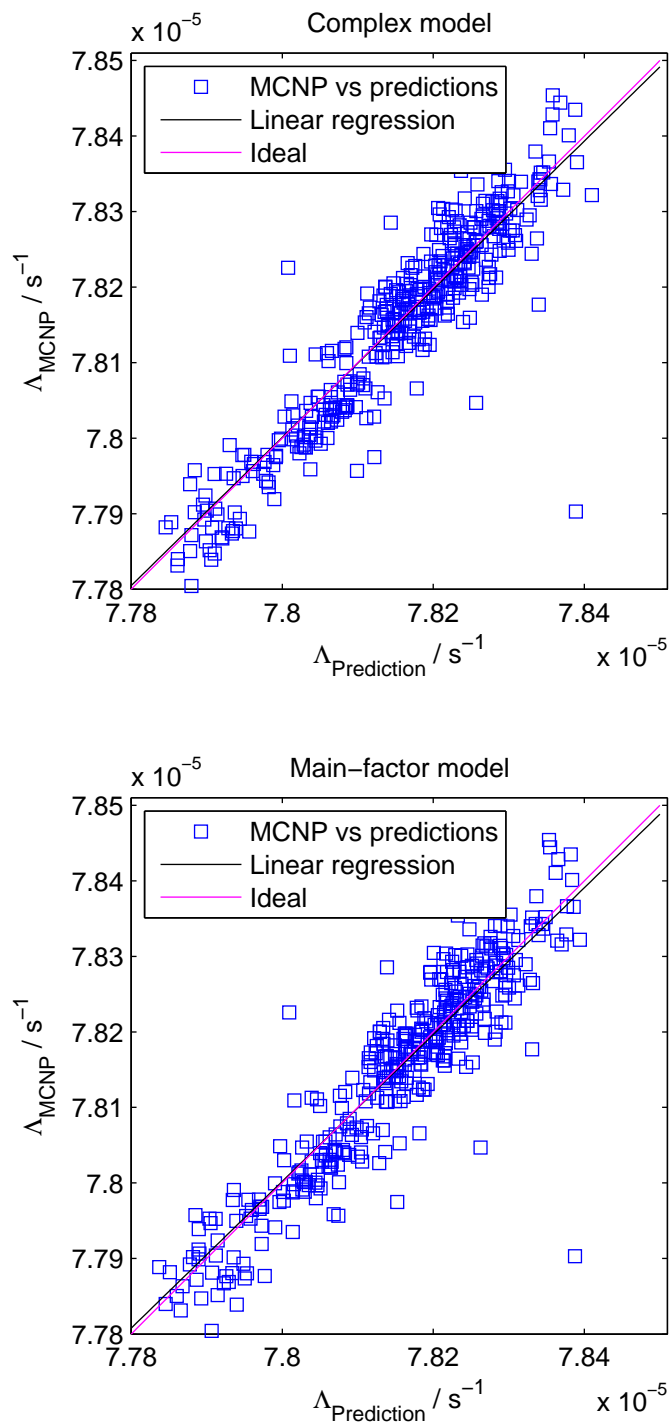
Figure 5.3: Cross validations for Λ

Furthemore, since both the definitions of ρ and Λ are directly correlated to the k_{eff}, Λ can be written as a functional of ρ as shown in Eq. 5.7.

$$\Lambda = l_p(1 - \rho \cdot \beta) \tag{5.7}$$

Where ρ is a function of the proposed parameters and in units of \$. The comparison between Λ from the main-factor regression model and the functional of ρ is performed and shown in Figure 5.4.
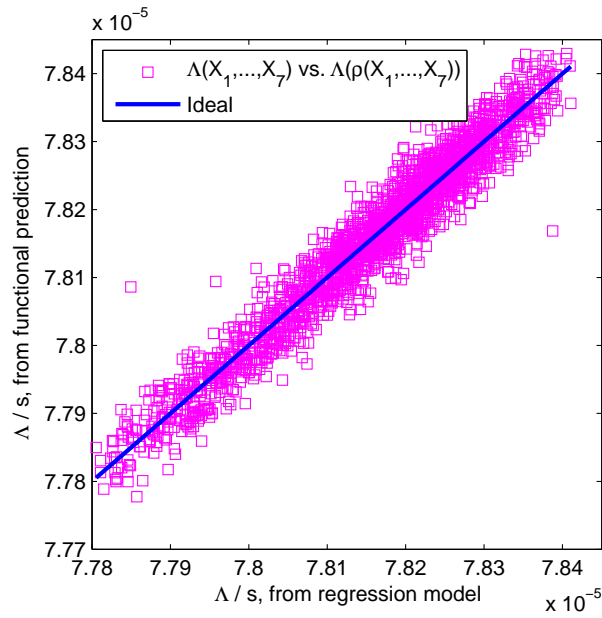
Figure 5.4: $\Lambda(\rho(X_1, \cdots, X_7))$ vs. $\Lambda(X_1, \cdots, X_7)$

From Figure 5.4, one would observe that the predicted Λ from the functional

is consistent with the Λ from regression models. This somewhat demonstrates the reasonableness of the methodology. And it also shows that predictions are robust.

$$\text{Cross validations for } \beta_{\text{eff}}$$

For β_{eff}, only one model was concerned. However, the regression model, illustrated in both Eq. 5.8 Table B.11, with an R^2 of 0.00242 would be really poor in predicting, as the cross validation shown in Figure 5.5.

$$\beta_{\text{eff}} = 7.6169 \times 10^{-3} + 1.0998 \times 10^{-5} X_3 \tag{5.8}$$
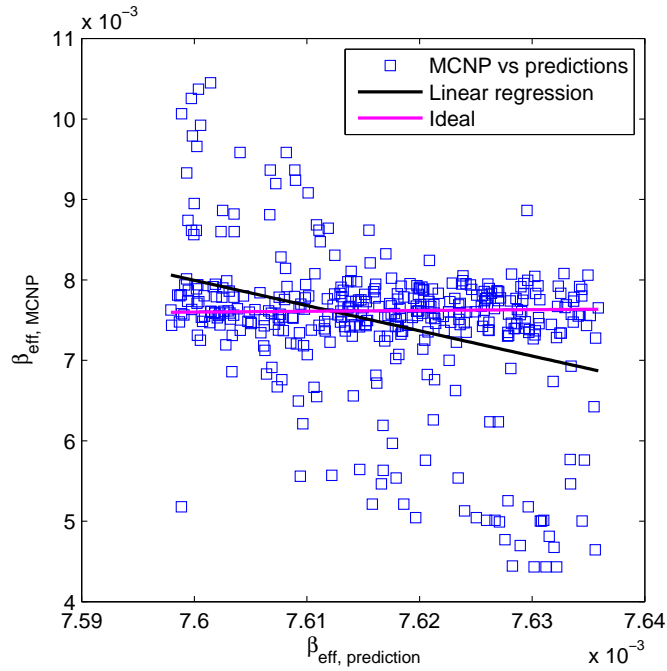
Figure 5.5: Cross validations for β_{eff}

From Figure 5.5, we noticed that outliers are not randomly distributed. The pre-

dictions underestimate for the outliers in the left part of Figure 5.5 and overestimate for the outliers. We thus hypothesized the exponential nonlinearity and performed log-transformation for the β_{eff} and analyzed the log-transformed β_{eff}. ANOVA results indicate that $\ln \beta_{\text{eff}}$ is sensitive to X_2, X_3, and X_2^3. Cross-validation for the scaled β_{eff} was performed, as shown in Figure 5.6 and the regression model is shown in Eq. 5.9.

$$\ln \left(\beta_{\text{eff}} \right) = -4.8878 - 1.9967 \times 10^{-3} X_2 + 1.4436 \times 10^{-3} X_3$$
$$+ 8.784 \times 10^{-4} X_2^3$$

$$(5.9)$$
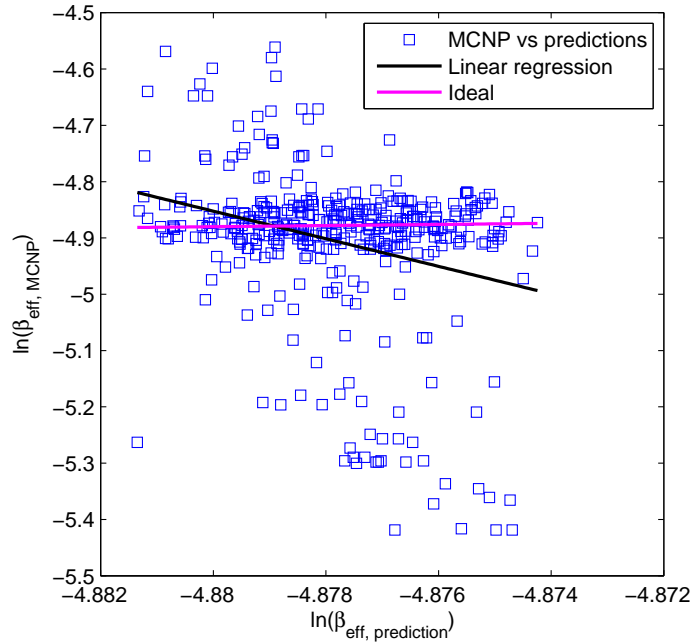
Figure 5.6: Cross validations for $\ln \beta_{\text{eff}}$

Results from the cross validation for $\ln(\beta_{\text{eff}})$ indicate that the nonlinearity is not resolved by the logarithm transformation. We believe there must be some unrecognized nonlnearity for β_{eff}.

Cross validations for α_T^{Fuel}

Though Badea, et al. studied the effects on dk_{eff}/dT from shifting the optical phonon of H in ZrH_x, no quantification of the effects was done [1].

We obtained the α_T^{Fuel} for fuel temperature of 300 K via 5.4 by setting the two fuel temperature required in 5.4 at 300 K and 400 K, respectively. We regressed the α_T^{Fuel} (equivalent to dk_{eff}/dT) with factors indicated by the ANOVA table in this thesis. The regression coefficients in the training part for α_T^{Fuel} are listed in Table B.14 and Table B.15, respectively. The main-factor model is shown in Eq. 5.10. And the testing results for both models are illustrated in Figure 5.7. Results show that though the R^2 are not large, the predictions of α_T^{Fuel} still have the trend of fitting the simulation results.

$$
\begin{aligned}
\alpha_T^{\text{Fuel}} = &- 7.1100 \times 10^{-3} - 3.8141 \times 10^{-5} X_2 + 1.9761 \times 10^{-4} X_3 \\
&- 3.7494 \times 10^{-5} X_3^2 + 3.4709 \times 10^{-5} X_3^3
\end{aligned}
\tag{5.10}
$$
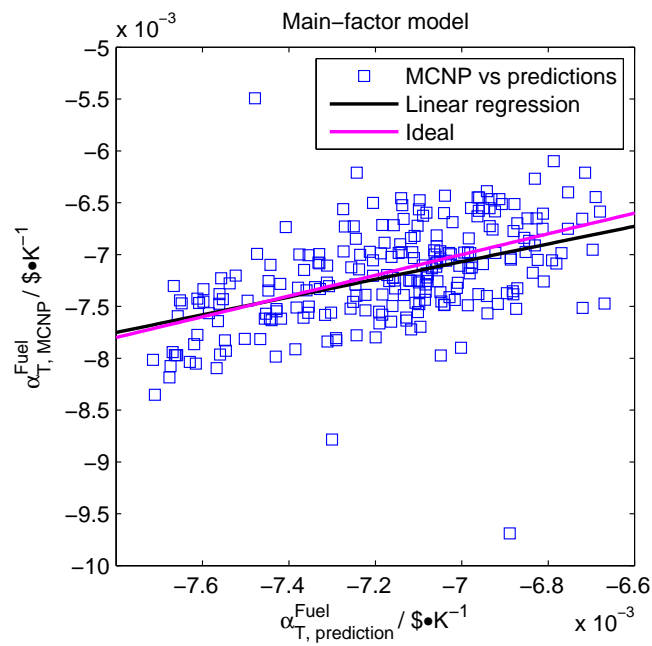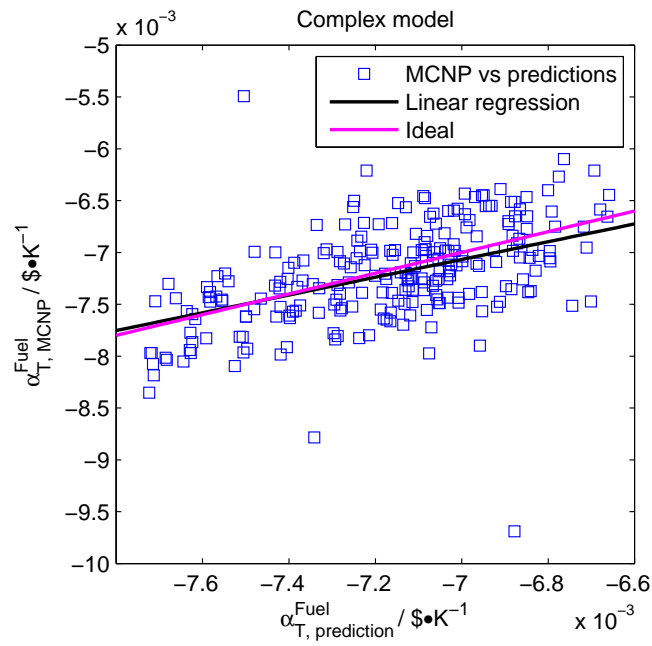
Figure 5.7: Cross validations for α_T^{Fuel}

5.2.3   Score Estimations

With the score estimations, we would estimate the dependencies of each QOI on the main factors. The difference from scores in Chapter 4 is that the simulation model changes from a simple lattice to a complicated full-core such that the dependencies might change.

Score for ρ

The score distributions for ρ on the main-factor plane are shown in Figure 5.8. Recall the scores for ρ shown by 4.5 on Page 48. In Figure 4.5, scores for ρ in IKE and ENDF cases have distinct distributions on the main-factor plane. While in Figure 5.8, the high scores locate at similar regions in both IKE and ENDF cases. A possible reason is the difference of system complexity. System complexity for the single lattice model is much lower than the full-core model. Once the phonon spectra change, e.g. from ENDF to IKE, noticable variations of sensitive QOIs, e.g. ρ would be induced for the lattice model since there are not as many components as the full-core model to provide resistance for sensitive QOIs, e.g. ρ, change.

One could exclude the reason of the accuracy of MCNP simulations for the lattice model since the difference of k_{eff} from these two references is 67 pcm which has been beyond the standard deviation of 23 pcm for each case.

Another observation for Figure 5.8 is that reactivity is more sensitive to X_3 than to X_2. Actually, this phenomena is also indicated by the regressions in the cross-validations. For ρ, the regression coefficient of X_3 has a larger magnitude than that of X_2. Moreover, the existence of higher order terms X_3^2 and X_3^3 would also indicate the higher sensitivity of X_3.
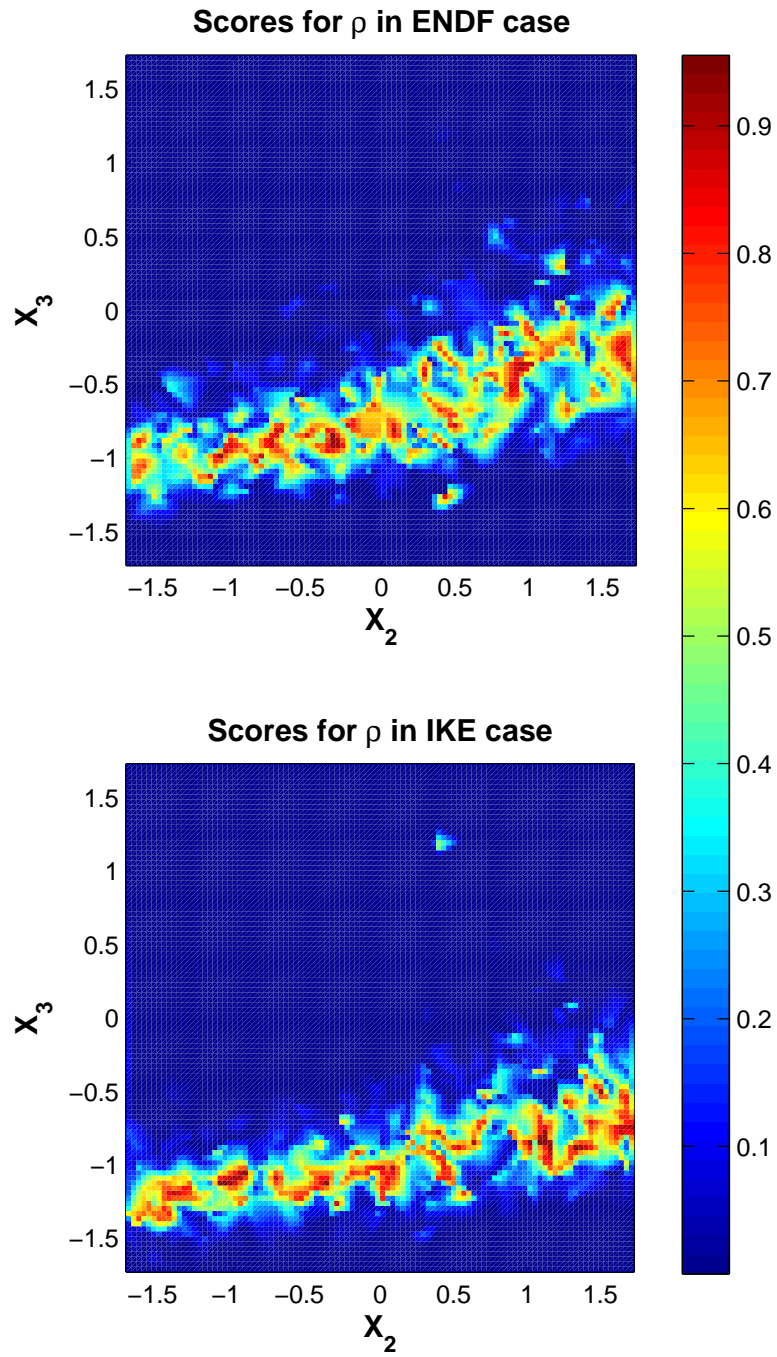
Figure 5.8: Score distribution on main-factor plane for ρ

Figure 5.9 illustrates the score distributions for Λ on the main-factor plane. The dependencies of Λ on the main factors are similar to ρ. We found that the prompt neutron lifetimes for all realizations from MCNP simulations behaves as constants with noise. Therefore, from the definition of Λ shown in 5.2, one could easily point out the similarities between Λ and ρ that they are both the hyperbolic functions of k_{eff} (if the prompt neutron lifetime is treated as a constant).

And this is consistent with results in the regression test on Page 60. Both of these results show that simple mathematical treatments to the physical models propagating through data processing and simulations make different QOIs still numerically correlated as implied by their physical correlations as illustrated in Eq. 5.7. This fact demonstrates the reasonableness of the parameterized model one more time.

Results also indicate that not only the reactivity, but there might also be several other QOIs are sensitive to the proposed parameters. This implies that we may implement the calibrations based on several different QOI score results to narrow the parameter ranges down.
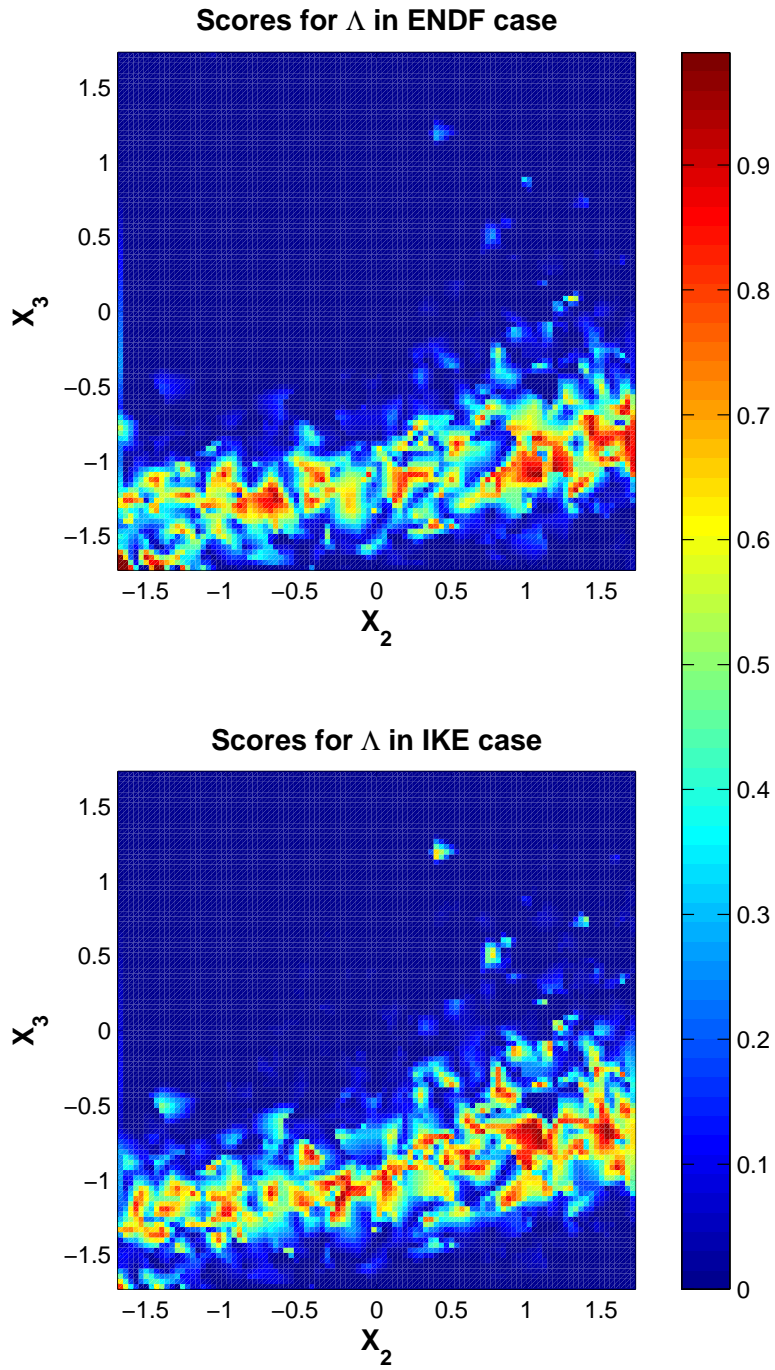
Figure 5.9: Score distribution on main-factor plane for Λ

Score for β_{eff}

Figure 5.10 illustrates the score distributions for β_{eff} on the main-factor plane. We noticed that the scores behave uniformly low on the main-factor plane in both IKE and ENDF cases. Different from the high-score uniform distributions on the main-factor plane, the low scores might indicate that the β_{eff} varies a lot implying the existence of some other unrecognized nonlinearities, which is consistent with the observations from the cross-validations for both β_{eff} and $\ln(\beta_{\text{eff}})$.

From the cross validation part, we observed that the β_{eff} has non-physical values. It means either there are some serious problems in the scattering kernel or the phonon spectrum models, or some problems occur to the result calculations.

The possible way for the parameterized model affect the β_{eff} is to affect the upscattering from thermal part to epithermal and fast neutrons. However, the expectations for the β_{eff} are values varying around the reference values. Therefore neither the lower bound of 0.004 nor the upper bound of 0.011 are reasonable.

Suggestions for the future work for β_{eff} are:

1. Increase the MCNP simulations accuracies, i.e. use more particles when running MCNP;

2. Check all possible issues of current simulation output files, including the cases indexing, etc.
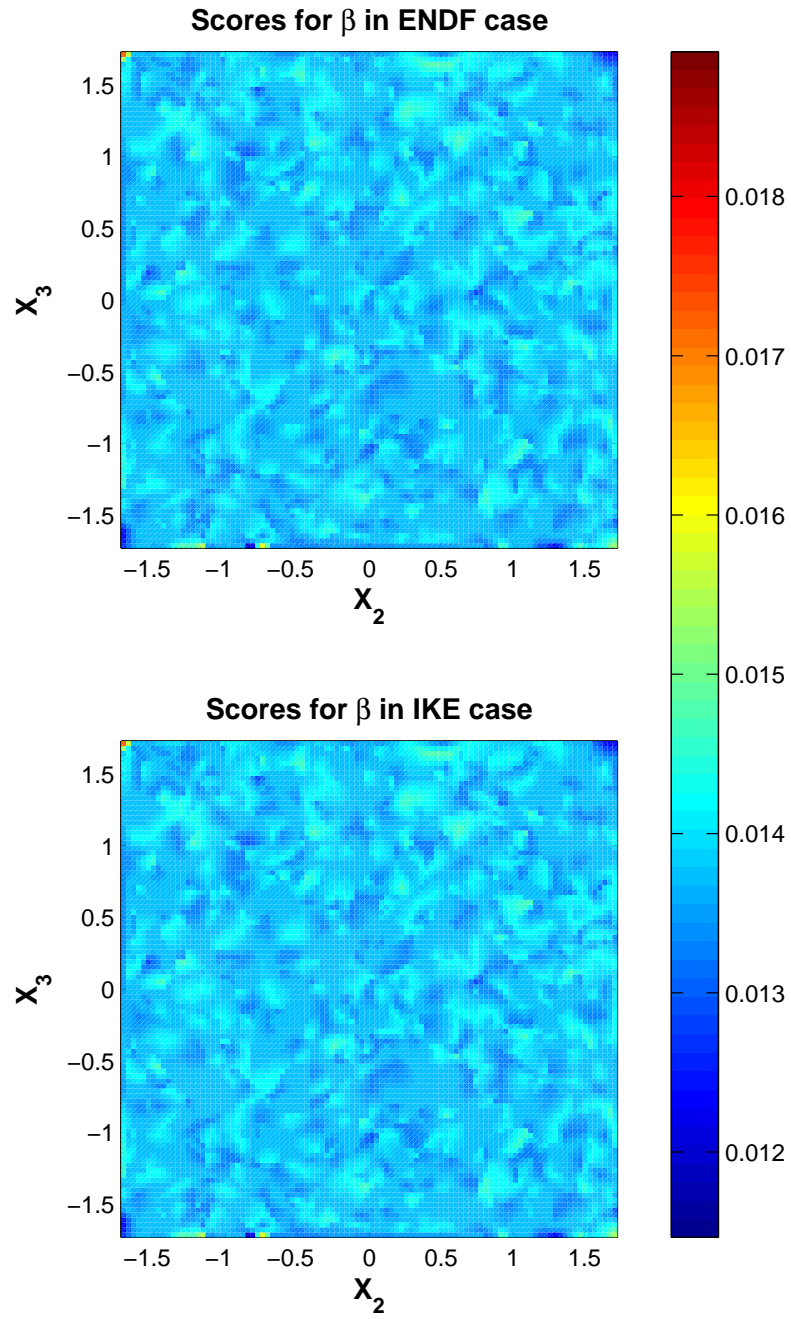
Figure 5.10: Score distribution on main-factor plane for β_{eff}

Score for α_T^{Fuel}

Figure 5.11 illustrates the score distributions for α_T^{Fuel} on the main-factor plane. The scores in the ENDF case show some ranges of main factors that could make this QOI from the parameterized models close to the one from ENDF. Similar phenomena can be observed in the IKE case, though the score distributions for these cases are distinct. Acutally, he IKE model presents a α_T^{Fuel} of -0.0082 \$/K and the ENDF model presents a α_T^{Fuel} of -0.0077 \$/K. The parameterized model presents α_T^{Fuel} ranging from $[-8.5 \times 10^{-3}, \ -6 \times 10^{-3}]$ \$/K. This could explain the distinction of the score distributions.

The different high score regions indicate that the α_T^{Fuel} is appropriate for calibrations. An important phenomenon is that the high score regions for both cases are different from the scores for reactivity. If the differences are not induced by the criticality accuracy or the statistical errors from Monte Carlo simulations, the scores for α_T^{Fuel} would probably help narrow down the parameter ranges.

Though the score estimations show different parameter preferences, one must be cautious when using α_T^{Fuel} to carry out the calibration. Cross validation results could only predict the trend of α_T^{Fuel}, and we also observe that the high score regions are widely distributed on main-factor plane. These results indicate that the accuracy of the criticality calculations would not be enough to preserve the accuracy of α_T^{Fuel}. More total numbers of neutrons must be used in MCNP simulations to get accurate α_T^{Fuel} to do the calibrations in the future.
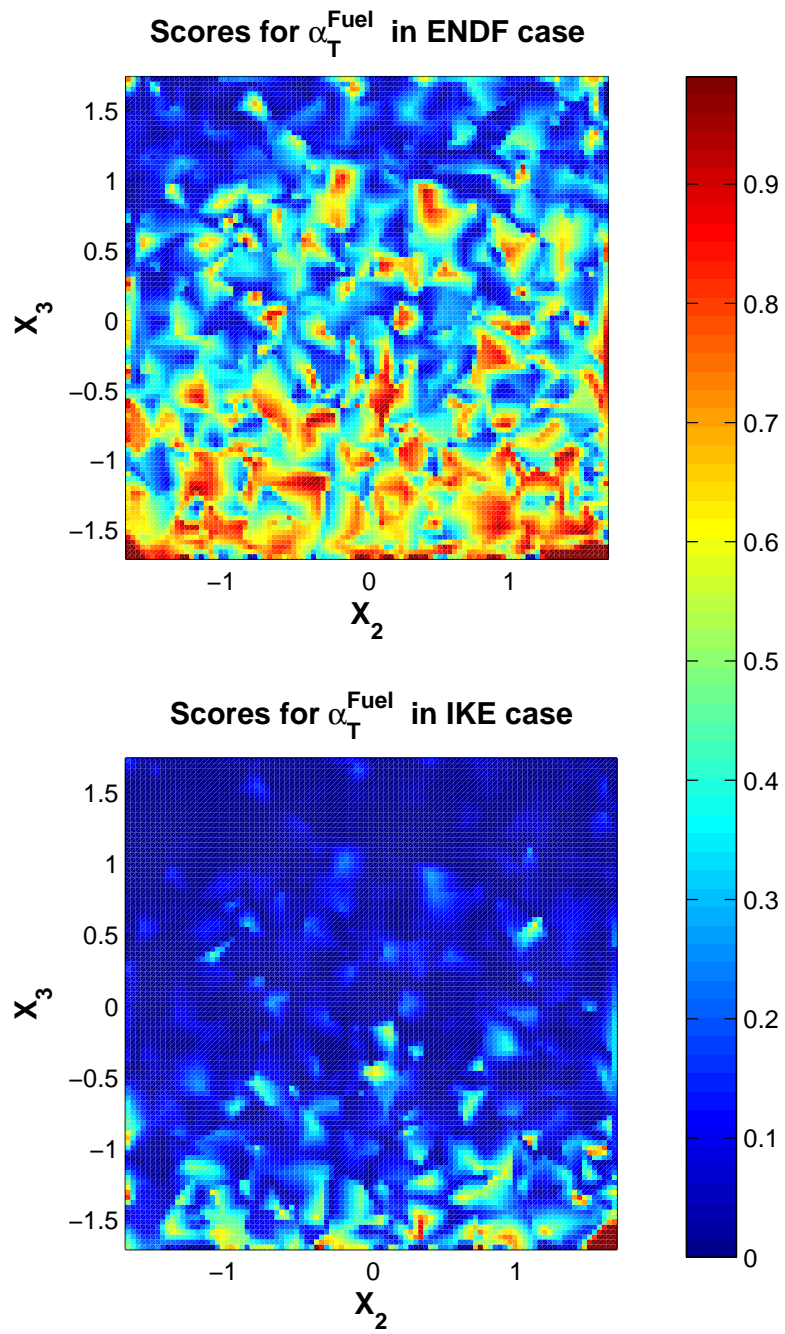
Figure 5.11: Score distribution on main-factor plane for α_T^{Fuel}

5.3 Ex-core Detectors Absorption Rate

5.3.1 MCNP Settings

Ex-core detectors are implemented outside the core as shown in Figure 5.12. The structure of the detectors are basically cylinders with cetral void filled with thin working gas. The height of the detectors are the same as the core. The thickness is 0.04 cm and the outer diameter is 2.54 cm. The detector material is 20 %enriched boron coated on the inner wall. The thickness of the coating is 0.00005 cm. This design is referred to an optimized design of GE boron lined detector by McKinny, et al. [9].
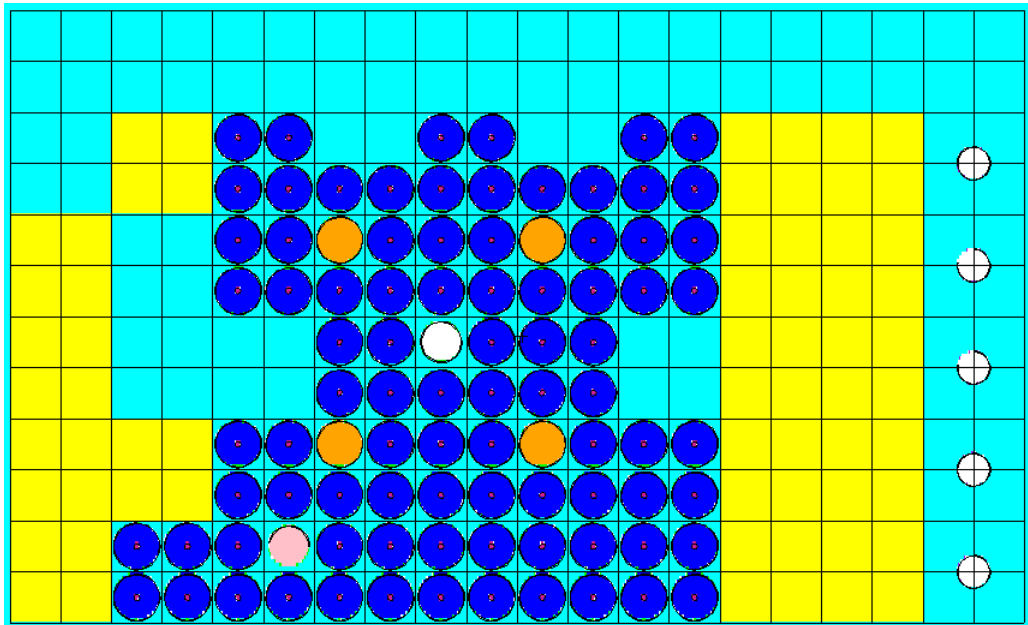
Figure 5.12: MCNP geometry with ex-core detectors

The kcode card is:

```
kcode 70000 1 30 270.
```

73

Which means 70000 neutrons are tracked in a cycle and there are 270 cycles in total. Thus, 1.89×10^7 neutrons per simulation are tracked in total. This configuration presented 21 pcm for the standard deviation of k_{eff}.

100 sets of parameters were generated via LHS design and the corresponding thermal scattering cross sections were produced.

5.3.2 Analyses for Detector Material Absorption Rate

In this section, analyses for the detector material absorption rate R_{abs} are performed. The analysis procedure is only applied to the detector on the topright part of Figure5.12 as an example.

The ANOVA was performed and results are shown in Table 16. And as implied by the ANOVA table, the important factors, X_3, X_1X_3, X_2X_5, X_5^2 and X_2^3, were selected to do the cross-validations.

In the cross-validations, 88 cases were used in the training set and 12 sets were used in the test set. The results are shown in Figure 5.13 and the regression model is presented by Eq. 5.11

$$
\begin{aligned}
R_{\text{abs}} = & 3.6246 \times 10^{-4} + 9.1332 \times 10^{-7} X_1 X_3 - 5.4516 \times 10^{-7} X_2 X_5 \\
& + 7.2104 \times 10^{-7} X_5^2 + 1.4926 \times 10^{-7} X_2^3
\end{aligned}
\tag{5.11}
$$

The R^2 is 0.173.
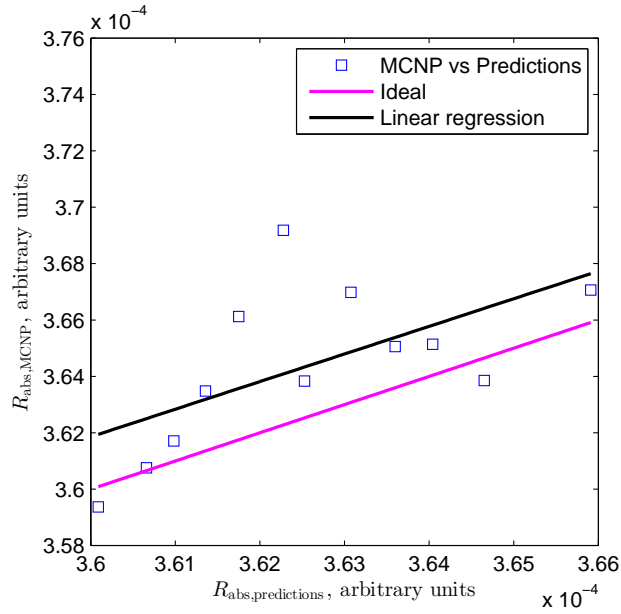
Figure 5.13: Cross-validations for ex-core detector material absorption rate R_{abs}

5.3.3 Results Implications

From the cross validations, though there are three outliers, we still observe nine predictions of R_{abs} have agreement with the simulation results. This might imply the feasibility of regressions applied for the R_{abs}. We plan to run much more than 100 MCNP simulations and will do the regressions taking the factors into account and expect good agreement between R_{abs} from the regressions and the ones from the simulations.

VI. CONCLUSION AND FUTURE WORK

In this study, seven parameters were proposed to construct the parameterized phonon spectra for H and Zr in ZrH_x.

6.1 Code Validity

We developed a code to process the multigroup thermal scattering cross sections for ZrH_x with the parameterized phonon spectra. The input of the code is only the seven-parameter set, which characterizes the phonon spectra, by default. The code-to-code comparisons show results from our code with a common set of parameters have good agreement with from NJOY in the testing cases. The analytical benchmarks show higher accuracy than NJOY.

6.2 Methodology Validity

In the simulation part, the strategy of performing the research using NJOY-MCNP with generated phonon spectra given parameters was proved to be feasible and effective.

Through the analyses, the combination of ANOVA, regression and score estimation is demonstrated to be appropriate for this UQ study. One can know the importance of the parameters for the QOIs through ANOVA. Regression could be applied with cross validation to provide reasonable explicit relationships between the QOIs and the important parameters (interactions and high order terms included) suggested by ANOVA. And score estimations would help one choose parameters to fit for the reference thermal scattering data.

6.3   Sensitivities of QOIs

Several QOIs were investigated in this thesis. In the study of lattice model of the TRIGA reactor, ρ is sensitive to the parameters, especially the main factors b, the branching ratio of acoustic phonon of H in ZrH_x, and p, the optical phonon peak position of H in ZrH_x. Score estimation also shows dependency of ρ on the main factors. While FRD is insensitive to any proposed parameters.

In the investigation of full-core TRIGA reactor model, ρ, Λ and α_T^{Fuel} are sensitive to the parameters. Explicit relationships were established for predicting QOIs if parameters are given. Good agreement are shown with simulation results in the testing part of the cross validations.

β_{eff} varies a lot, and the appropriate explicit relationship between β_{eff} and the parameters cannot be established. The behavior of β_{eff} is more random, instead of constant as in the case of FRD. We did logarithm transformation to β_{eff}, and analyzed $\ln(\beta_{\text{eff}})$ and found that explicit parameters cannot be established, also. We believe there being some unrecognized nonlinearities resulting in the variations of β_{eff}.

We investigated the absorption rate of the ex-core detector material. The results might indicate some sensitivity of the absorption rate of ex-core detectors. However, the sample size is small, which might not be enough to demonstrate the sensitivity. More simulation results are needed to reveal the relationship between this QOI and the proposed scattering model.

6.4   Directions for Future Work

One would be interested in the model applying in the near-critical states and supercritical states. QOIs like ρ, α_T^{Fuel}, etc. in the near-critical state will be investigated. We will also include the in-core detector and absorption in the detector materials

will be tallied. The sensitivity of the absorption rate of the in-core detectors to the parameters will be investigated.

Those significant high order terms in the regression models might be overestimated since there might be interdependencies between the high order factors e.g. X_3^2 and the corresponding low order terms e.g. X_3. Therefore, the orthogonalizations will be performed in the analysis in the future to avoid the overestimations of the significance of those high order terms.

The analyses of β_{eff} indicate regression might be inappropriate for the analyses for some sensitive QOIs. Emulators, e.g. Gaussian process, Bayesian multivariate automatic regression splines (BMARS), etc., would be applied in the analysis of QOIs.

Furthermore, as part of the current research plan, the time dependent behaviour of a TRIGA reactor during pulses will be investigated by simulations with transport codes coupled with thermal-hydraulics simulations.

We expect to find more QOIs sensitive to the parameters with the mothodology that combines ANOVA and cross-validation based on regressions. The score estimation developed in this thesis is expected to apply in calibrations with those sensitive QOIs for the corresponding experimental data as references. Appropriate parameter sets are thereafter expected to be calibrated to construct phonon spectra for Zr and H in ZrH_x in the TRIGA reactor at Texas A&M University. This would be expected to improve the simulation accuracy of the TRIGA reactor.

REFERENCES

[1] M. D. R. Badea and C. H. M. Broeders. On the Impact of Phonon Spectrum Shifts of the Hydrogen Binding in ZrH. In *International Conference on Nuclear Data for Science and Technology 2007*, number 242, 2008.

[2] G. I. Bell and S. Glasstone. *Nuclear Reactor Theory*. Krieger Pub Co, Princeton, NJ, 3rd edition, 1985.

[3] A. C. Evans, D. N. Timms, J. Mayers, and S. M. Bennington. Neutron-Scattering Study of the Impulse Approximation in ZrH_2. *Phys. Rev. B*, 53:3023–3031, Feb. 1996.

[4] O. K. Harling and L. C. Clune. Structure in the Neutron Scattering Spectra of Zirconium Hydride. *Physical Review B*, 4(8):923–934, 1971.

[5] The MathWorks Inc. anova1, one-way analysis of variance. `http://www.mathworks.com/help/stats/anova1.html`. [Online; accessed 10-Oct.-2013].

[6] R. E. MacFarlane. New Thermal Neutron Scattering Files for ENDF/B-VI, Release 2. Technical Report LA-12639-MS(ENDF 356), Los Alamos National Laboratory, Los Alamos, NM, 1994.

[7] S. S. Malik, D. C. Rorer, and G. Brunhart. Optical-Phonon Structure and Precision Neutron Total Cross Section Measurements of Zirconium Hydride. *J. Phys. F: Met. Phys*, 14:73–81, 1984.

[8] M. Mattes and J. Keinert. Thermal Netron Scattering Data for the Moderator Materials H_2O, D_2O and ZrH_x in ENDF-6 Format and as ACE Library for MCNP(X) Code. Technical Report INDC(NDS)-0470, Institue for Nuclear Technology and Energy System (IKE)-University of Stuttgart, 2005.

[9] K. S. McKinny, T. R. Anderson, and N. H. Johnson. Optimization of Coating in Boron-10 Lined Proportional Counters. *Nuclear Science, IEEE Transactions on*, 60(2):860–863, 2013.

[10] Texas A&M University Nuclear Science Center. Safety Analysis Report. Technical Report 05000128, Nuclear Science Center, Texas A&M University, 2011.

[11] T. J. Santner, B. J. Williams, and W. Notz. *The Design and Analysis of Computer Experiments*. Springer Series in Statistics. Springer, New York, NY, 2003.

[12] E. L. Slaggie. Central Force Lattice Dynamical Model for Zirconium Hydride. *J. Phys. Chem. Solids*, 29:923–934, 1968.

[13] D. D. Wackerly, W. Mendenhall, and R. L. Scheaffer. *Mathematical Statistics with Applications*. Cengage Learning Inc., Belmont, CA, 7th edition, 2008.

[14] E. W. Weisstein. ANOVA. `http://mathworld.wolfram.com/ANOVA.html`, 2008. [Online; accessed 10-Oct.-2013].

[15] Wikipedia. Analysis of Variance — Wikipedia, The Free Encyclopedia. `http://en.wikipedia.org/wiki/Analysis_of_variance`. [Online; accessed 9-Oct.-2013].

APPENDIX A

ANOVA TABLES AND REGRESSION COEFFICIENT TABLES FOR QOIS

FOR CHAPTER 4

This appendix is for the lists of ANOVA tables and regression models in Chapter 4. For reactivity, ρ, there are an ANOVA table for all parameters, the first order interactions and high order terms of the main factors and two regression coefficients tables. Also, the μ_i and σ_i, $i = 1, \cdots, 7$ are given for every QOI. For FRD, the only difference is that there is only one regression table given.

Table A.1: ANOVA table for ρ

Observations	SumSq	DF	MeanSq	F	pValue
X1	4.3157e-02	1	4.3157e-02	7.4067e+01	1.2053e-17
X2	1.8942e+00	1	1.8942e+00	3.2509e+03	0.0000e+00
X3	2.4572e+00	1	2.4572e+00	4.2171e+03	0.0000e+00
X4	1.1572e-02	1	1.1572e-02	1.9860e+01	8.6432e-06
X5	6.2433e-02	1	6.2433e-02	1.0715e+02	1.0826e-24
X6	1.2760e-02	1	1.2760e-02	2.1900e+01	3.0013e-06
X7	1.2812e-02	1	1.2812e-02	2.1989e+01	2.8661e-06
X1:X2	7.6809e-03	1	7.6809e-03	1.3182e+01	2.8740e-04
X1:X3	1.0444e-03	1	1.0444e-03	1.7925e+00	1.8073e-01
X2:X3	1.2723e-02	1	1.2723e-02	2.1835e+01	3.1036e-06
X1:X4	7.6349e-04	1	7.6349e-04	1.3103e+00	2.5243e-01
X2:X4	1.4403e-02	1	1.4403e-02	2.4718e+01	7.0132e-07

X3:X4	1.9297e-05	1	1.9297e-05	3.3118e-02	8.5561e-01
X1:X5	2.2233e-04	1	2.2233e-04	3.8158e-01	5.3681e-01
X2:X5	1.9577e-04	1	1.9577e-04	3.3598e-01	5.6220e-01
X3:X5	9.6157e-04	1	9.6157e-04	1.6503e+00	1.9902e-01
X4:X5	1.0712e-04	1	1.0712e-04	1.8384e-01	6.6812e-01
X1:X6	1.2507e-04	1	1.2507e-04	2.1466e-01	6.4317e-01
X2:X6	8.2479e-08	1	8.2479e-08	1.4155e-04	9.9051e-01
X3:X6	2.9720e-03	1	2.9720e-03	5.1006e+00	2.3990e-02
X4:X6	6.7955e-03	1	6.7955e-03	1.1663e+01	6.4627e-04
X5:X6	3.6438e-05	1	3.6438e-05	6.2536e-02	8.0255e-01
X1:X7	7.9190e-04	1	7.9190e-04	1.3591e+00	2.4379e-01
X2:X7	1.4984e-05	1	1.4984e-05	2.5717e-02	8.7260e-01
X3:X7	1.2852e-04	1	1.2852e-04	2.2057e-01	6.3864e-01
X4:X7	5.5825e-04	1	5.5825e-04	9.5809e-01	3.2775e-01
X5:X7	2.0862e-04	1	2.0862e-04	3.5804e-01	5.4964e-01
X6:X7	1.3513e-03	1	1.3513e-03	2.3192e+00	1.2789e-01
X1^2	2.4654e-04	1	2.4654e-04	4.2312e-01	5.1544e-01
X2^2	2.5239e-03	1	2.5239e-03	4.3316e+00	3.7497e-02
X3^2	6.4131e-02	1	6.4131e-02	1.1006e+02	2.6210e-25
X4^2	2.2586e-04	1	2.2586e-04	3.8763e-01	5.3360e-01
X5^2	5.1840e-06	1	5.1840e-06	8.8970e-03	9.2486e-01
X6^2	4.2071e-05	1	4.2071e-05	7.2203e-02	7.8817e-01
X7^2	5.6382e-05	1	5.6382e-05	9.6764e-02	7.5577e-01
X2^3	4.3877e-04	1	4.3877e-04	7.5304e-01	3.8559e-01

X3^3	2.9596e-02	1	2.9596e-02	5.0794e+01	1.2831e-12
X3^4	1.2236e-04	1	1.2236e-04	2.1000e-01	6.4680e-01
Error	1.7253e+00	2961	5.8267e-04	1.0000e+00	5.0000e-01

Table A.2: μ_i and σ_i of the parameters for ρ

	P_1	P_2	P_3	P_4	P_5	P_6	P_7
μ_i	28.0000	0.006880	137.0000	20.0000	20.0000	0.5750	2.4000
σ_i	1.7323	0.002373	2.8872	2.3098	2.3098	0.1011	0.2310

Table A.3: The regression coefficients of the complex model for ρ, $R^2 = 0.714$

Observations	Estimate	SE	tStat	pValue
(Intercept)	3.2565e+01	0.00093	3.4993e+04	0.0000e+00
X1	3.7932e-03	0.0005	7.5668e+00	5.4286e-14
X2	2.5036e-02	0.0005	4.9709e+01	0.0000e+00
X3	-2.1153e-02	0.00126	-1.6803e+01	5.7363e-60
X4	-1.6889e-03	0.00051	-3.3238e+00	9.0145e-04
X5	-4.5655e-03	0.0005	-9.1098e+00	1.6996e-19
X6	1.7922e-03	0.0005	3.5638e+00	3.7266e-04
X7	-1.9880e-03	0.0005	-3.9787e+00	7.1352e-05
X1:X2	1.4731e-03	0.0005	2.9541e+00	3.1670e-03
X2:X3	-1.8838e-03	0.0005	-3.7374e+00	1.9029e-04
X2:X4	-2.3263e-03	0.00051	-4.5682e+00	5.1703e-06
X4:X6	1.6992e-03	0.0005	3.3737e+00	7.5348e-04
X2^2	-7.9164e-04	0.00056	-1.4042e+00	1.6038e-01
X3^2	5.2777e-03	0.00056	9.3472e+00	2.0013e-20
X3^3	-4.3281e-03	0.00065	-6.6932e+00	2.7129e-11

Table A.4: The regression coefficients of the main-factor model for ρ, $R^2 = 0.687$

Observations	Estimate	SE	tStat	pValue
(Intercept)	3.2564e+01	0.00078	4.1606e+04	0.0000e+00
X2	2.5229e-02	0.00052	4.8139e+01	0.0000e+00
X3	-2.1105e-02	0.00131	-1.6088e+01	2.2165e-55
X2:X3	-1.8799e-03	0.00052	-3.5945e+00	3.3157e-04
X3^2	5.2404e-03	0.00059	8.9059e+00	1.0234e-18
X3^3	-4.3131e-03	0.00067	-6.4064e+00	1.7874e-10

Table A.5: ANOVA table for FRD

Observations	SumSq	DF	MeanSq	F	pValue
X1	3.8566e-08	1	3.8566e-08	1.1103e-02	9.1609e-01
X2	4.1069e-04	1	4.1069e-04	1.1823e+02	4.9639e-27
X3	4.2850e-04	1	4.2850e-04	1.2336e+02	4.1419e-28
X4	2.2559e-06	1	2.2559e-06	6.4945e-01	4.2037e-01
X5	1.2204e-05	1	1.2204e-05	3.5133e+00	6.0975e-02
X6	4.4256e-10	1	4.4256e-10	1.2741e-04	9.9099e-01
X7	5.5125e-06	1	5.5125e-06	1.5870e+00	2.0785e-01
X1:X2	2.2749e-06	1	2.2749e-06	6.5493e-01	4.1842e-01
X1:X3	8.8224e-06	1	8.8224e-06	2.5399e+00	1.1111e-01
X2:X3	4.9682e-06	1	4.9682e-06	1.4303e+00	2.3181e-01
X1:X4	6.3990e-07	1	6.3990e-07	1.8422e-01	6.6780e-01
X2:X4	1.8111e-06	1	1.8111e-06	5.2141e-01	4.7030e-01
X3:X4	6.0750e-07	1	6.0750e-07	1.7489e-01	6.7583e-01

X1:X5	3.6508e-09	1	3.6508e-09	1.0510e-03	9.7414e-01
X2:X5	2.7816e-07	1	2.7816e-07	8.0079e-02	7.7721e-01
X3:X5	2.6575e-06	1	2.6575e-06	7.6506e-01	3.8182e-01
X4:X5	1.3803e-06	1	1.3803e-06	3.9736e-01	5.2850e-01
X1:X6	7.9263e-07	1	7.9263e-07	2.2819e-01	6.3290e-01
X2:X6	4.4713e-06	1	4.4713e-06	1.2873e+00	2.5665e-01
X3:X6	1.7269e-07	1	1.7269e-07	4.9716e-02	8.2357e-01
X4:X6	1.6087e-06	1	1.6087e-06	4.6312e-01	4.9622e-01
X5:X6	2.5791e-08	1	2.5791e-08	7.4251e-03	9.3134e-01
X1:X7	1.3271e-06	1	1.3271e-06	3.8205e-01	5.3655e-01
X2:X7	5.4699e-06	1	5.4699e-06	1.5747e+00	2.0962e-01
X3:X7	7.6469e-07	1	7.6469e-07	2.2015e-01	6.3896e-01
X4:X7	4.9664e-06	1	4.9664e-06	1.4298e+00	2.3189e-01
X5:X7	1.1925e-06	1	1.1925e-06	3.4330e-01	5.5798e-01
X6:X7	1.3589e-06	1	1.3589e-06	3.9122e-01	5.3171e-01
X1^2	6.3977e-06	1	6.3977e-06	1.8418e+00	1.7484e-01
X2^2	5.7556e-06	1	5.7556e-06	1.6570e+00	1.9811e-01
X3^2	8.1474e-06	1	8.1474e-06	2.3456e+00	1.2575e-01
X4^2	4.5605e-06	1	4.5605e-06	1.3129e+00	2.5196e-01
X5^2	5.5621e-06	1	5.5621e-06	1.6013e+00	2.0582e-01
X6^2	7.4002e-07	1	7.4002e-07	2.1305e-01	6.4442e-01
X7^2	1.0106e-06	1	1.0106e-06	2.9093e-01	5.8966e-01
X2^3	2.0798e-06	1	2.0798e-06	5.9876e-01	4.3911e-01
X3^3	7.0318e-07	1	7.0318e-07	2.0244e-01	6.5279e-01

X3^4	3.7418e-06	1	3.7418e-06	1.0772e+00	2.9940e-01
Error	1.0285e-02	2961	3.4735e-06	1.0000e+00	5.0000e-01

Table A.6: μ_i and σ_i of the parameters for FRD

	P_1	P_2	P_3	P_4	P_5	P_6	P_7
μ_i	28.0000	0.006880	137.0000	20.0000	20.0000	0.5750	2.4000
σ_i	1.7323	0.002373	2.8872	2.3098	2.3098	0.1011	0.2310

Table A.7: The regression coefficients of the regression model for FRD, $R^2 = 0.0944$

Observations	Estimate	SE	tStat	pValue
(Intercept)	4.2117e+00	4e-005	1.1018e+05	0.0000e+00
X2	4.2499e-04	4e-005	1.1085e+01	7.0113e-28
X3	-4.4680e-04	4e-005	-1.1639e+01	1.6927e-30

APPENDIX B

ANOVA TABLES AND REGRESSION COEFFICIENT TABLES FOR QOIS FOR CHAPTER 5

This appendix is for the lists of ANOVA tables and regression models in Chapter 5. Except for the delayed neutron fraction, β, every QOI has an ANOVA table for all parameters, the first order interactions and high order terms of the main factors and two regression coefficients tables. Also the μ_i and σ_i, $i = 1, \cdots, 7$ are given for every QOI. For β, the only difference is that there is only one regression table given.

Table B.1: ANOVA table for ρ

Observations	SumSq	DF	MeanSq	F	pValue
X1	3.9619e-02	1	3.9619e-02	2.7701e+01	1.5722e-07
X2	2.9535e+00	1	2.9535e+00	2.0650e+03	8.0972e-308
X3	3.8214e+01	1	3.8214e+01	2.6718e+04	0.0000e+00
X4	2.7398e-02	1	2.7398e-02	1.9156e+01	1.2682e-05
X5	1.8896e-01	1	1.8896e-01	1.3212e+02	1.2485e-29
X6	5.4276e-02	1	5.4276e-02	3.7949e+01	8.8032e-10
X7	2.0832e-02	1	2.0832e-02	1.4566e+01	1.3960e-04
X1:X2	5.4640e-03	1	5.4640e-03	3.8203e+00	5.0778e-02
X1:X3	3.9393e-04	1	3.9393e-04	2.7543e-01	5.9977e-01
X2:X3	1.8838e-03	1	1.8838e-03	1.3171e+00	2.5126e-01
X1:X4	1.1950e-04	1	1.1950e-04	8.3552e-02	7.7257e-01
X2:X4	7.8336e-04	1	7.8336e-04	5.4771e-01	4.5934e-01

X3:X4	2.5937e-08	1	2.5937e-08	1.8134e-05	9.9660e-01
X1:X5	2.0296e-03	1	2.0296e-03	1.4190e+00	2.3371e-01
X2:X5	3.1527e-03	1	3.1527e-03	2.2043e+00	1.3779e-01
X3:X5	7.9574e-06	1	7.9574e-06	5.5637e-03	9.4055e-01
X4:X5	5.8533e-03	1	5.8533e-03	4.0925e+00	4.3210e-02
X1:X6	1.1841e-03	1	1.1841e-03	8.2789e-01	3.6300e-01
X2:X6	5.9762e-04	1	5.9762e-04	4.1784e-01	5.1809e-01
X3:X6	9.0792e-03	1	9.0792e-03	6.3480e+00	1.1831e-02
X4:X6	5.4654e-03	1	5.4654e-03	3.8213e+00	5.0748e-02
X5:X6	6.3573e-03	1	6.3573e-03	4.4449e+00	3.5134e-02
X1:X7	3.5198e-03	1	3.5198e-03	2.4610e+00	1.1687e-01
X2:X7	4.3302e-03	1	4.3302e-03	3.0276e+00	8.2019e-02
X3:X7	7.7875e-03	1	7.7875e-03	5.4449e+00	1.9728e-02
X4:X7	7.2958e-06	1	7.2958e-06	5.1011e-03	9.4307e-01
X5:X7	9.8721e-04	1	9.8721e-04	6.9024e-01	4.0619e-01
X6:X7	2.5576e-04	1	2.5576e-04	1.7882e-01	6.7243e-01
X1^2	4.3505e-04	1	4.3505e-04	3.0418e-01	5.8134e-01
X2^2	4.9143e-03	1	4.9143e-03	3.4360e+00	6.3942e-02
X3^2	1.4400e+00	1	1.4400e+00	1.0068e+03	2.1510e-178
X4^2	3.9641e-06	1	3.9641e-06	2.7716e-03	9.5802e-01
X5^2	1.4628e-02	1	1.4628e-02	1.0228e+01	1.4056e-03
X6^2	1.3602e-03	1	1.3602e-03	9.5100e-01	3.2959e-01
X7^2	6.6418e-04	1	6.6418e-04	4.6438e-01	4.9566e-01
X2^3	9.2273e-04	1	9.2273e-04	6.4515e-01	4.2195e-01

X3^3	3.5543e-01	1	3.5543e-01	2.4851e+02	8.8721e-53
X3^4	5.4010e-06	1	5.4010e-06	3.7763e-03	9.5101e-01
Error	2.7790e+00	1943	1.4302e-03	1.0000e+00	5.0000e-01

Table B.2: μ_i and σ_i of the parameters for ρ

	P_1	P_2	P_3	P_4	P_5	P_6	P_7
μ_i	27.9995	0.006896	137.0060	19.9904	20.0180	0.5745	2.4027
σ_i	1.7253	0.002362	5.7685	2.3096	2.3080	0.1006	0.2317

Table B.3: The regression coefficients of the complex model for ρ, $R^2 = 0.926$

Observations	Estimate	SE	tStat	pValue
(Intercept)	-3.8500e+00	0.00106	-3.6353e+03	0.0000e+00
X1	4.6048e-03	0.00105	4.3863e+00	1.2295e-05
X2	3.8782e-02	0.00105	3.6789e+01	2.6565e-214
X3	-1.4037e-01	0.00105	-1.3367e+02	0.0000e+00
X4	-4.4286e-03	0.00106	-4.1855e+00	3.0029e-05
X5	-9.6944e-03	0.00107	-9.0991e+00	2.6783e-19
X6	6.0522e-03	0.00106	5.7058e+00	1.3809e-08
X7	-4.5449e-03	0.00106	-4.2827e+00	1.9579e-05
X1:X2	1.7597e-03	0.00104	1.6879e+00	9.1636e-02
X3:X6	-1.4010e-03	0.00105	-1.3361e+00	1.8173e-01
X5:X6	-2.1443e-03	0.00107	-1.9986e+00	4.5824e-02
X5:X7	-1.2179e-03	0.00105	-1.1610e+00	2.4581e-01

Table B.4: The regression coefficients of the main-factor model for ρ, $R^2 = 0.955$

Observations	Estimate	SE	tStat	pValue
(Intercept)	-3.8793e+00	0.00124	-3.1230e+03	0.0000e+00
X2	3.9815e-02	0.00082	4.8634e+01	2.8226e-316
X3	-1.0728e-01	0.00204	-5.2557e+01	0.0000e+00
X3^2	2.9019e-02	0.00091	3.1724e+01	2.5798e-171
X3^3	-1.8434e-02	0.00103	-1.7857e+01	4.1610e-65

Table B.5: ANOVA tables for Λ

Observations	SumSq	DF	MeanSq	F	pValue
X1	4.5210e-14	1	4.5210e-14	2.2708e+01	2.0262e-06
X2	2.6206e-12	1	2.6206e-12	1.3163e+03	1.6232e-220
X3	2.8916e-11	1	2.8916e-11	1.4524e+04	0.0000e+00
X4	5.5332e-15	1	5.5332e-15	2.7791e+00	9.5661e-02
X5	2.0735e-13	1	2.0735e-13	1.0415e+02	7.4188e-24
X6	8.8739e-14	1	8.8739e-14	4.4571e+01	3.1912e-11
X7	2.6681e-14	1	2.6681e-14	1.3401e+01	2.5818e-04
X1:X2	1.2510e-14	1	1.2510e-14	6.2834e+00	1.2268e-02
X1:X3	9.1081e-16	1	9.1081e-16	4.5747e-01	4.9889e-01
X2:X3	4.5619e-15	1	4.5619e-15	2.2913e+00	1.3026e-01
X1:X4	2.0754e-15	1	2.0754e-15	1.0424e+00	3.0739e-01
X2:X4	2.4024e-15	1	2.4024e-15	1.2066e+00	2.7213e-01
X3:X4	6.4688e-16	1	6.4688e-16	3.2490e-01	5.6874e-01
X1:X5	4.7199e-15	1	4.7199e-15	2.3706e+00	1.2380e-01
X2:X5	1.2987e-15	1	1.2987e-15	6.5229e-01	4.1939e-01
X3:X5	5.9046e-17	1	5.9046e-17	2.9657e-02	8.6329e-01
X4:X5	9.3172e-15	1	9.3172e-15	4.6797e+00	3.0642e-02
X1:X6	1.2275e-15	1	1.2275e-15	6.1655e-01	4.3243e-01
X2:X6	1.7289e-15	1	1.7289e-15	8.6835e-01	3.5153e-01
X3:X6	1.6301e-14	1	1.6301e-14	8.1873e+00	4.2636e-03
X4:X6	7.4708e-15	1	7.4708e-15	3.7524e+00	5.2878e-02
X5:X6	9.7256e-15	1	9.7256e-15	4.8849e+00	2.7210e-02

X1:X7	1.6700e-15	1	1.6700e-15	8.3879e-01	3.5986e-01
X2:X7	3.2219e-15	1	3.2219e-15	1.6183e+00	2.0349e-01
X3:X7	1.0809e-14	1	1.0809e-14	5.4291e+00	1.9906e-02
X4:X7	8.5268e-17	1	8.5268e-17	4.2828e-02	8.3607e-01
X5:X7	1.5779e-15	1	1.5779e-15	7.9250e-01	3.7345e-01
X6:X7	5.9148e-16	1	5.9148e-16	2.9708e-01	5.8578e-01
X1^2	1.6494e-17	1	1.6494e-17	8.2845e-03	9.2749e-01
X2^2	2.7737e-15	1	2.7737e-15	1.3931e+00	2.3802e-01
X3^2	1.3789e-12	1	1.3789e-12	6.9260e+02	8.2066e-131
X4^2	9.4072e-16	1	9.4072e-16	4.7249e-01	4.9192e-01
X5^2	2.2751e-14	1	2.2751e-14	1.1427e+01	7.3822e-04
X6^2	3.2342e-16	1	3.2342e-16	1.6245e-01	6.8696e-01
X7^2	6.7103e-17	1	6.7103e-17	3.3704e-02	8.5436e-01
X2^3	1.4723e-17	1	1.4723e-17	7.3947e-03	9.3148e-01
X3^3	3.5801e-13	1	3.5801e-13	1.7982e+02	2.7986e-39
X3^4	7.4204e-15	1	7.4204e-15	3.7270e+00	5.3684e-02
Error	3.8685e-12	1943	1.9910e-15	1.0000e+00	5.0000e-01

Table B.6: μ_i and σ_i of the parameters for Λ

	P_1	P_2	P_3	P_4	P_5	P_6	P_7
μ_i	27.9995	0.006896	137.0060	19.9904	20.0180	0.5745	2.4027
σ_i	1.7253	0.002362	5.7685	2.3096	2.3080	0.1006	0.2317

Table B.7: The regression coefficients of the complex model for Λ, $R^2 = 0.918$

Observations	Estimate	SE	tStat	pValue
(Intercept)	7.8186e-05	2e-009	4.1149e+04	0.0000e+00
X1	-5.6817e-09	1e-009	-5.6973e+00	1.4508e-08
X2	-3.6687e-08	1e-009	-3.6616e+01	1.0206e-212
X3	8.8026e-08	2e-009	3.5223e+01	8.8944e-201
X5	9.8241e-09	1e-009	9.7096e+00	1.1016e-21
X6	-6.7186e-09	1e-009	-6.6654e+00	3.6432e-11
X7	4.5572e-09	1e-009	4.5179e+00	6.7132e-06
X1:X2	-2.8341e-09	1e-009	-2.8569e+00	4.3341e-03
X4:X5	-2.0703e-09	1e-009	-2.0397e+00	4.1545e-02
X3:X6	1.1844e-09	1e-009	1.1887e+00	2.3474e-01
X5:X6	1.6466e-09	1e-009	1.6077e+00	1.0810e-01
X3:X7	-1.1664e-09	1e-009	-1.1655e+00	2.4400e-01
X3^2	-2.7859e-08	1e-009	-2.4912e+01	1.0438e-115
X5^2	-3.1002e-09	1e-009	-2.7336e+00	6.3358e-03
X3^3	1.8937e-08	1e-009	1.4967e+01	1.9148e-47

Table B.8: The regression coefficients of the main-factor model for Λ, $R^2 = 0.907$

Observations	Estimate	SE	tStat	pValue
(Intercept)	7.8183e-05	2e-009	4.8400e+04	0.0000e+00
X2	-3.7219e-08	1e-009	-3.4960e+01	7.8133e-199
X3	8.7285e-08	3e-009	3.2883e+01	4.0955e-181
X3^2	-2.7854e-08	1e-009	-2.3415e+01	2.4733e-104
X3^3	1.9164e-08	1e-009	1.4275e+01	1.4248e-43

Table B.9: ANOVA table for β_{eff}

Observations	SumSq	DF	MeanSq	F	pValue
X1	7.2932e-07	1	7.2932e-07	3.3831e+00	6.6021e-02
X2	7.4796e-07	1	7.4796e-07	3.4696e+00	6.2659e-02
X3	5.7652e-06	1	5.7652e-06	2.6743e+01	2.5638e-07
X4	1.8484e-08	1	1.8484e-08	8.5742e-02	7.6969e-01
X5	7.3251e-08	1	7.3251e-08	3.3979e-01	5.6002e-01
X6	1.7007e-08	1	1.7007e-08	7.8893e-02	7.7883e-01
X7	7.1664e-09	1	7.1664e-09	3.3243e-02	8.5535e-01
X1:X2	1.8929e-07	1	1.8929e-07	8.7808e-01	3.4884e-01
X1:X3	1.0086e-07	1	1.0086e-07	4.6784e-01	4.9406e-01
X2:X3	4.7086e-07	1	4.7086e-07	2.1842e+00	1.3960e-01
X1:X4	2.0301e-07	1	2.0301e-07	9.4172e-01	3.3196e-01
X2:X4	8.9771e-08	1	8.9771e-08	4.1642e-01	5.1880e-01
X3:X4	3.9755e-07	1	3.9755e-07	1.8441e+00	1.7462e-01
X1:X5	1.7115e-08	1	1.7115e-08	7.9391e-02	7.7815e-01

X2:X5	2.7110e-08	1	2.7110e-08	1.2576e-01	7.2291e-01
X3:X5	1.9587e-08	1	1.9587e-08	9.0858e-02	7.6312e-01
X4:X5	6.3559e-07	1	6.3559e-07	2.9483e+00	8.6128e-02
X1:X6	2.6639e-10	1	2.6639e-10	1.2357e-03	9.7196e-01
X2:X6	3.1147e-09	1	3.1147e-09	1.4448e-02	9.0434e-01
X3:X6	7.9455e-08	1	7.9455e-08	3.6857e-01	5.4386e-01
X4:X6	1.0281e-07	1	1.0281e-07	4.7689e-01	4.8992e-01
X5:X6	3.5017e-07	1	3.5017e-07	1.6244e+00	2.0264e-01
X1:X7	1.8030e-07	1	1.8030e-07	8.3635e-01	3.6056e-01
X2:X7	7.7998e-08	1	7.7998e-08	3.6181e-01	5.4757e-01
X3:X7	1.0742e-06	1	1.0742e-06	4.9831e+00	2.5710e-02
X4:X7	3.8082e-07	1	3.8082e-07	1.7665e+00	1.8397e-01
X5:X7	2.1579e-09	1	2.1579e-09	1.0010e-02	9.2032e-01
X6:X7	2.4724e-07	1	2.4724e-07	1.1469e+00	2.8434e-01
X1^2	1.3836e-08	1	1.3836e-08	6.4179e-02	8.0003e-01
X2^2	2.4912e-09	1	2.4912e-09	1.1556e-02	9.1440e-01
X3^2	3.0473e-07	1	3.0473e-07	1.4136e+00	2.3461e-01
X4^2	6.6796e-07	1	6.6796e-07	3.0985e+00	7.8522e-02
X5^2	1.0576e-06	1	1.0576e-06	4.9058e+00	2.6883e-02
X6^2	1.0632e-07	1	1.0632e-07	4.9320e-01	4.8259e-01
X7^2	1.8364e-07	1	1.8364e-07	8.5185e-01	3.5614e-01
X2^3	1.2272e-06	1	1.2272e-06	5.6924e+00	1.7134e-02
X3^3	3.2593e-09	1	3.2593e-09	1.5119e-02	9.0215e-01
X3^4	4.9368e-08	1	4.9368e-08	2.2901e-01	6.3232e-01

Error	4.1671e-04	1933	2.1558e-07	1.0000e+00	5.0000e-01

Table B.10: μ_i and σ_i of the parameters for β_{eff}

	P_1	P_2	P_3	P_4	P_5	P_6	P_7
μ_i	27.9969	0.006889	137.0097	19.9961	20.0148	0.5746	2.4025
σ_i	1.7244	0.002362	5.7721	2.3072	2.3078	0.1005	0.2317

Table B.11: The regression coefficients of the regression model for β_{eff}, $R^2 = 0.00242$

Observations	Estimate	SE	tStat	pValue
(Intercept)	7.6169e-03	6e-006	1.3418e+03	0.0000e+00
X3	1.0998e-05	6e-006	1.9564e+00	5.0597e-02

Table B.12: ANOVA table for α_T^{Fuel}

Observations	SumSq	DF	MeanSq	F	pValue
X1	1.4983E-08	1	1.4983E-08	9.1474E-02	7.6236E-01
X2	1.5736E-06	1	1.5736E-06	9.6069E+00	1.9844E-03
X3	7.2338E-05	1	7.2338E-05	4.4163E+02	1.6422E-83
X4	1.1453E-09	1	1.1453E-09	6.9920E-03	9.3337E-01

X5	1.4902E-06	1	1.4902E-06	9.0976E+00	2.6143E-03
X6	1.7586E-07	1	1.7586E-07	1.0736E+00	3.0034E-01
X7	6.7031E-07	1	6.7031E-07	4.0924E+00	4.3303E-02
X1:X2	2.8236E-07	1	2.8236E-07	1.7238E+00	1.8946E-01
X1:X3	1.4247E-08	1	1.4247E-08	8.6983E-02	7.6810E-01
X2:X3	2.4990E-08	1	2.4990E-08	1.5257E-01	6.9616E-01
X1:X4	1.6644E-09	1	1.6644E-09	1.0162E-02	9.1972E-01
X2:X4	1.2888E-08	1	1.2888E-08	7.8685E-02	7.7914E-01
X3:X4	1.5968E-08	1	1.5968E-08	9.7488E-02	7.5492E-01
X1:X5	8.9047E-09	1	8.9047E-09	5.4364E-02	8.1568E-01
X2:X5	1.8442E-07	1	1.8442E-07	1.1259E+00	2.8887E-01
X3:X5	1.9218E-07	1	1.9218E-07	1.1733E+00	2.7894E-01
X4:X5	4.4366E-07	1	4.4366E-07	2.7086E+00	1.0008E-01
X1:X6	8.7754E-10	1	8.7754E-10	5.3575E-03	9.4166E-01
X2:X6	2.7819E-07	1	2.7819E-07	1.6984E+00	1.9275E-01
X3:X6	3.8468E-07	1	3.8468E-07	2.3485E+00	1.2567E-01
X4:X6	2.6273E-07	1	2.6273E-07	1.6040E+00	2.0559E-01
X5:X6	2.1960E-07	1	2.1960E-07	1.3407E+00	2.4715E-01
X1:X7	3.9807E-07	1	3.9807E-07	2.4303E+00	1.1928E-01
X2:X7	3.7582E-07	1	3.7582E-07	2.2944E+00	1.3011E-01
X3:X7	1.3210E-07	1	1.3210E-07	8.0650E-01	3.6934E-01
X4:X7	1.7527E-07	1	1.7527E-07	1.0700E+00	3.0115E-01
X5:X7	7.8251E-08	1	7.8251E-08	4.7774E-01	4.8959E-01
X6:X7	3.8073E-07	1	3.8073E-07	2.3244E+00	1.2763E-01

X1^2	2.0332E-07	1	2.0332E-07	1.2413E+00	2.6545E-01
X2^2	4.0465E-08	1	4.0465E-08	2.4705E-01	6.1926E-01
X3^2	2.1709E-06	1	2.1709E-06	1.3254E+01	2.8382E-04
X4^2	9.4277E-08	1	9.4277E-08	5.7558E-01	4.4820E-01
X5^2	1.8829E-08	1	1.8829E-08	1.1496E-01	7.3463E-01
X6^2	4.0004E-07	1	4.0004E-07	2.4423E+00	1.1837E-01
X7^2	4.0972E-08	1	4.0972E-08	2.5014E-01	6.1707E-01
X2^3	3.4262E-07	1	3.4262E-07	2.0918E+00	1.4836E-01
X3^3	8.7175E-07	1	8.7175E-07	5.3222E+00	2.1229E-02
X3^4	3.4820E-07	1	3.4820E-07	2.1258E+00	1.4510E-01
Error	1.9279E-04	1177	1.6380E-07	1.0000E+00	5.0000E-01

Table B.13: μ_i and σ_i of the parameters for α_T^{Fuel}

	P_1	P_2	P_3	P_4	P_5	P_6	P_7
μ_i	27.9569	0.006911	136.8930	19.9243	20.0225	0.5745	2.4077
σ_i	1.7033	0.002388	5.794	2.3121	2.3036	0.1013	0.2326

Table B.14: The regression coefficients of the complex model for α_T^{Fuel}, $R^2 = 0.358$

Observations	Estimate	SE	tStat	pValue
(Intercept)	-7.1098E-03	1.7661E-05	-4.0258E+02	0.0000E+00
X2	-3.9322E-05	1.1609E-05	-3.3872E+00	7.3458E-04
X3	1.9418E-04	2.8944E-05	6.7088E+00	3.3400E-11
X5	-3.4500E-05	1.1753E-05	-2.9354E+00	3.4097E-03
X7	-6.3935E-06	1.1685E-05	-5.4716E-01	5.8439E-01
X3^2	-3.7721E-05	1.3085E-05	-2.8826E+00	4.0312E-03
X3^3	3.6113E-05	1.4718E-05	2.4536E+00	1.4321E-02

Table B.15: The regression coefficients of the main-factor model for α_T^{Fuel}, $R^2 = 0.352$

Observations	Estimate	SE	tStat	pValue
(Intercept)	-7.1100E-03	1.7723E-05	-4.0118e+02	0.0000e+00
X2	-3.8141E-05	1.1643E-05	-3.2759e+00	1.0906E-03
X3	1.9761E-04	2.9023E-05	6.8088e+00	1.7254E-11
X3^2	-3.7494E-05	1.3131E-05	-2.8553e+00	4.3916E-03
X3^3	3.4709E-05	1.4762E-05	2.3513e+00	1.8907E-02

Table B.16: ANOVA table for R_{abs}

Observations	SumSq	DF	MeanSq	F	pValue
Observations	SumSq	DF	MeanSq	F	pValue

X1	5.3823e-12	1	5.3823e-12	6.1115e-01	4.3738e-01
X2	5.7282e-12	1	5.7282e-12	6.5043e-01	4.2309e-01
X3	7.5153e-11	1	7.5153e-11	8.5334e+00	4.8824e-03
X4	2.3469e-11	1	2.3469e-11	2.6648e+00	1.0774e-01
X5	2.4906e-12	1	2.4906e-12	2.8280e-01	5.9680e-01
X6	6.7848e-12	1	6.7848e-12	7.7040e-01	3.8354e-01
X7	1.1608e-11	1	1.1608e-11	1.3181e+00	2.5542e-01
X1:X2	5.5359e-12	1	5.5359e-12	6.2859e-01	4.3095e-01
X1:X3	4.0195e-11	1	4.0195e-11	4.5641e+00	3.6669e-02
X2:X3	2.5422e-12	1	2.5422e-12	2.8866e-01	5.9304e-01
X1:X4	5.5654e-12	1	5.5654e-12	6.3194e-01	4.2973e-01
X2:X4	1.5233e-11	1	1.5233e-11	1.7296e+00	1.9338e-01
X3:X4	2.5364e-12	1	2.5364e-12	2.8800e-01	5.9346e-01
X1:X5	1.8828e-12	1	1.8828e-12	2.1378e-01	6.4546e-01
X2:X5	3.1606e-11	1	3.1606e-11	3.5888e+00	6.2914e-02
X3:X5	6.1565e-14	1	6.1565e-14	6.9906e-03	9.3364e-01
X4:X5	3.5608e-12	1	3.5608e-12	4.0432e-01	5.2725e-01
X1:X6	1.5213e-12	1	1.5213e-12	1.7274e-01	6.7915e-01
X2:X6	5.6655e-14	1	5.6655e-14	6.4331e-03	9.3634e-01
X3:X6	5.5963e-12	1	5.5963e-12	6.3545e-01	4.2846e-01
X4:X6	7.3579e-15	1	7.3579e-15	8.3547e-04	9.7704e-01
X5:X6	2.0859e-12	1	2.0859e-12	2.3685e-01	6.2823e-01
X1:X7	6.0113e-12	1	6.0113e-12	6.8256e-01	4.1192e-01
X2:X7	8.8737e-13	1	8.8737e-13	1.0076e-01	7.5201e-01

X3:X7	2.7675e-11	1	2.7675e-11	3.1425e+00	8.1272e-02
X4:X7	9.8893e-12	1	9.8893e-12	1.1229e+00	2.9347e-01
X5:X7	1.4272e-12	1	1.4272e-12	1.6205e-01	6.8868e-01
X6:X7	4.5922e-14	1	4.5922e-14	5.2144e-03	9.4267e-01
X1^2	6.5999e-12	1	6.5999e-12	7.4940e-01	3.9006e-01
X2^2	1.9904e-12	1	1.9904e-12	2.2600e-01	6.3620e-01
X3^2	6.6064e-12	1	6.6064e-12	7.5014e-01	3.8983e-01
X4^2	1.0720e-11	1	1.0720e-11	1.2172e+00	2.7424e-01
X5^2	6.4917e-11	1	6.4917e-11	7.3712e+00	8.6078e-03
X6^2	1.5661e-11	1	1.5661e-11	1.7783e+00	1.8732e-01
X7^2	5.0348e-16	1	5.0348e-16	5.7169e-05	9.9399e-01
X2^3	4.9436e-11	1	4.9436e-11	5.6133e+00	2.1005e-02
X3^3	3.2414e-11	1	3.2414e-11	3.6805e+00	5.9735e-02
X3^4	3.0388e-14	1	3.0388e-14	3.4505e-03	9.5335e-01
Error	5.3722e-10	61	8.8069e-12	1.0000e+00	5.0000e-01

APPENDIX C

DERIVATIONS FOR THE "SCORE" USED IN CHAPTER 4 AND CHAPTER 5

In Chapter 4 and Chapter 5, we proposed a quantity named "score", which is the overlapped area between QOIs from the parameterized models and the reference QOIs. Note that quantities from MCNP simulations are given as normal distributions with a mean value and a standard deviation.

Here are the notations for this derivation:

1. $f_i(x)$ / $f_{ref}(x)$: Normal distributions for QOIs from parameterized models / references

2. μ_i / μ_{ref}: the means of QOIs from parameterized models / references.

3. σ_i / σ_{ref}: the standard deviations of QOIs from parameterized models / references.

With the notations above, the normal distributions can be given by:

$$f_i(x) = \frac{1}{\sqrt{2\pi}\sigma_i} \exp\left[-\frac{(x-\mu_i)^2}{2\sigma_i^2}\right], \tag{C.1}$$

and

$$f_{ref}(x) = \frac{1}{\sqrt{2\pi}\sigma_{ref}} \exp\left[-\frac{(x-\mu_{ref})^2}{2\sigma_{ref}^2}\right]. \tag{C.2}$$

We aim to find the cross point(s) of the two distributions, i.e. to solve Eq. C.3, so that we can calculate the overlapped area.

$$f_i(x) = f_{ref}(x) \quad \text{or} \quad \frac{1}{\sigma_i}\exp\left[-\frac{(x-\mu_i)^2}{2\sigma_i^2}\right] = \frac{1}{\sigma_{ref}}\exp\left[-\frac{(x-\mu_{ref})^2}{2\sigma_{ref}^2}\right]. \tag{C.3}$$

Rearrange Eq. C.4, one could get:

$$(\sigma_{\text{ref}}^2 - \sigma_{\text{i}}^2)x^2 - 2(\sigma_{\text{ref}}^2 \mu_{\text{i}} - \sigma_{\text{i}}^2 \mu_{\text{ref}})x + \sigma_{\text{ref}}^2 \mu_{\text{i}}^2 - \sigma_{\text{i}}^2 \mu_{\text{ref}}^2 - C_0 = 0, \qquad \text{(C.4)}$$

where

$$C_0 = 2\sigma_{\text{i}}^2 \sigma_{\text{ref}}^2 \log \frac{\sigma_{\text{ref}}}{\sigma_{\text{i}}}. \qquad \text{(C.5)}$$

The symbolic solution of Eq. C.4 would be:

$$x = \frac{(\sigma_{\text{ref}}^2 \mu_{\text{i}} - \sigma_{\text{i}}^2 \mu_{\text{ref}}) \pm \sqrt{\sigma_{\text{i}}^2 \sigma_{\text{ref}}^2 (\mu_{\text{i}} - \mu_{\text{ref}})^2 + C_0(\sigma_{\text{ref}}^2 - \sigma_{\text{i}}^2)}}{\sigma_{\text{ref}}^2 - \sigma_{\text{i}}^2}. \qquad \text{(C.6)}$$

That is,

$$x = \frac{(\sigma_{\text{ref}}^2 \mu_{\text{i}} - \sigma_{\text{i}}^2 \mu_{\text{ref}}) \pm \sigma_{\text{i}} \sigma_{\text{ref}} \sqrt{(\mu_{\text{i}} - \mu_{\text{ref}})^2 + 2\log \frac{\sigma_{\text{ref}}}{\sigma_{\text{i}}} (\sigma_{\text{ref}}^2 - \sigma_{\text{i}}^2)}}{\sigma_{\text{ref}}^2 - \sigma_{\text{i}}^2}. \qquad \text{(C.7)}$$

Since $\log \dfrac{\sigma_{\text{ref}}}{\sigma_{\text{i}}}$ and $(\sigma_{\text{ref}}^2 - \sigma_{\text{i}}^2)$ will have the same sign, Eq. C.7 always has real solutions.

C.1   If $\sigma_{\text{i}} = \sigma_{\text{ref}}$:

In this case, $C_0 = 0$ and the solution of Eq. C.4. will be:

$$x = \frac{\mu_{\text{i}} + \mu_{\text{ref}}}{2} \qquad \text{(C.8)}$$

Denote x by x_{cp}.

Since the solution is identical, there will be only one cross point for the two distributions, as shown in Figure C.1.

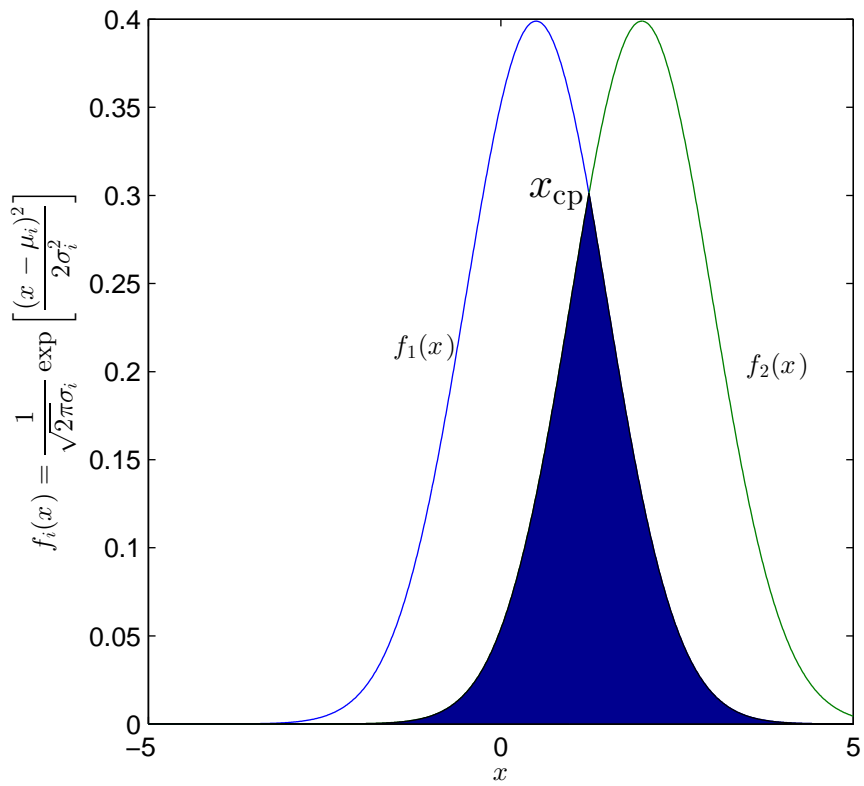Before calculating the score, one should determine which one of the $f_{\text{i}}(x)$ and fr

104

Figure C.1: An example of overlapped area of two normal distributions with equal σ.

is $f_1(x)$ to the left. Then the score can be given by:

$$\text{score} = \Phi(\hat{x_{cp}}^2) + \left[1 - \Phi(\hat{x_{cp}}^1)\right],\tag{C.9}$$

where Φ stands for cumulative standard normal distribution. $\hat{x_{cp}}^i,\ i = 1, 2$, is the standardized value for x_{cp} which is standardized with μ_i and $\sigma_i,\ i = 1, 2$. And the standardization is given by:

$$\hat{x_{cp}}^i = \frac{x_{cp} - \mu_i}{\sigma_i}.\tag{C.10}$$

The values of cumulative standard normal distribution at specific points can be given by function cdf in MATLAB.

C.2 If $\sigma_i \neq \sigma_{\text{ref}}$:

In this case, Eq. C.4 will have two solutions, denote the smaller one by $x_{cp,\ 1}$ and denote the larger one by $x_{cp,\ 2}$. There will be two cross points as shown in Figure C.2.

As previously discussed, one should determine which one between $f_i(x)$ and $f_{\text{ref}}(x)$ is $f_1(x)$ to the left. Then the score can be calculated by:

$$\text{score} = \Phi(\hat{x_{cp,\ 1}}^1) + \left[\Phi(\hat{x_{cp,\ 2}}^2) - \Phi(\hat{x_{cp,\ 1}}^2)\right] + \left[1 - \Phi(\hat{x_{cp,\ 2}}^1)\right],\tag{C.11}$$

where $\hat{x_{cp,\ j}}^i,\ i, j = 1, 2$ is the standardized value of $x_{cp,\ j}$, which is standardized by μ_i and σ_i. And the standardization is given by:

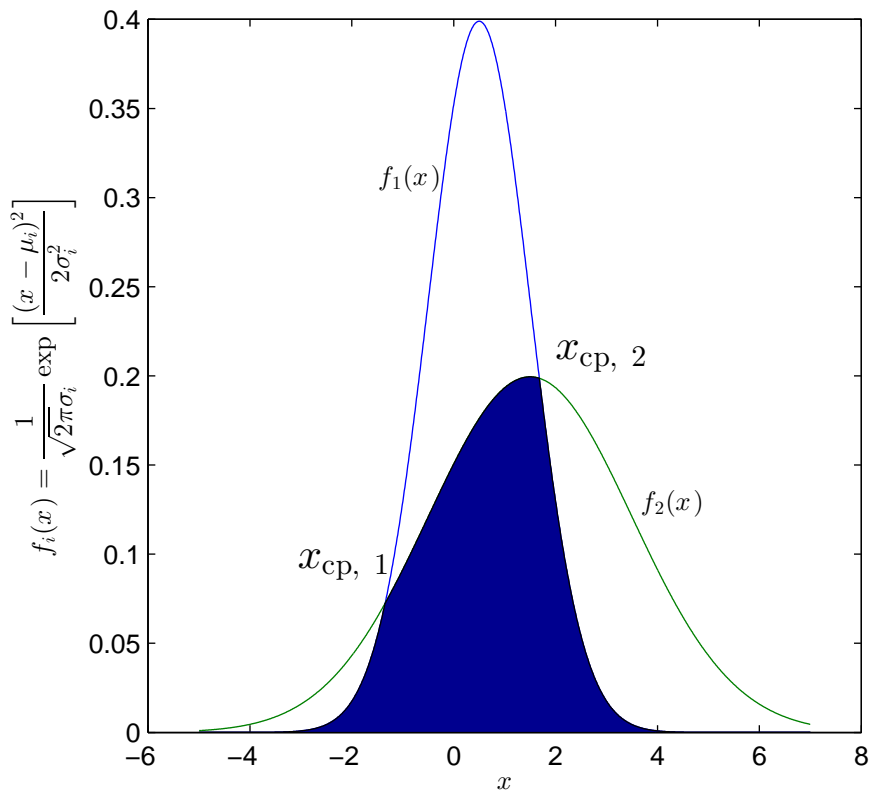$$\hat{x_{cp,\ j}}^i = \frac{x_{cp,\ j} - \mu_i}{\sigma_i}.\tag{C.12}$$

Figure C.2: An example of overlapped area of two normal distributions with distinct σ.